



Review

Recent Advancements in Applications of Graphene to Attain Next-Level Solar Cells

Sonal Santosh Bagade ¹, Shashidhar Patel ², M. M. Malik ³ and Piyush K. Patel ^{1,*}

¹ Renewable Energy Laboratory, Department of Physics, Maulana Azad National Institute of Technology, Bhopal 462003, India; sonalbagade87@gmail.com

² Government Polytechnic, Shahjahanpur 242001, India; shashi.bietce@gmail.com

³ Nanotechnology Research Laboratory, Department of Physics, Maulana Azad National Institute of Technology, Bhopal 462003, India; malikmm@manit.ac.in

* Correspondence: piyush.phy@manit.ac.in

Abstract: This paper presents an intensive review covering all the versatile applications of graphene and its derivatives in solar photovoltaic technology. To understand the internal working mechanism for the attainment of highly efficient graphene-based solar cells, graphene's parameters of control, namely its number of layers and doping concentration are thoroughly discussed. The popular graphene synthesis techniques are studied. A detailed review of various possible applications of utilizing graphene's attractive properties in solar cell technology is conducted. This paper clearly mentions its applications as an efficient transparent conducting electrode, photoactive layer and Schottky junction formation. The paper also covers advancements in the 10 different types of solar cell technologies caused by the incorporation of graphene and its derivatives in solar cell architecture. Graphene-based solar cells are observed to outperform those solar cells with the same configuration but lacking the presence of graphene in them. Various roles that graphene efficiently performs in the individual type of solar cell technology are also explored. Moreover, bi-layer (and sometimes, tri-layer) graphene is shown to have the potential to fairly uplift the solar cell performance appreciably as well as impart maximum stability to solar cells as compared to multi-layered graphene. The current challenges concerning graphene-based solar cells along with the various strategies adopted to resolve the issues are also mentioned. Hence, graphene and its derivatives are demonstrated to provide a viable path towards light-weight, flexible, cost-friendly, eco-friendly, stable and highly efficient solar cell technology.

Keywords: Dirac point; Fermi level; sheet resistance; transparency; work function



Citation: Bagade, S.S.; Patel, S.; Malik, M.M.; Patel, P.K. Recent Advancements in Applications of Graphene to Attain Next-Level Solar Cells. *C* **2023**, *9*, 70.
<https://doi.org/10.3390/c9030070>

Academic Editors: Vardan Apinyan, Tadeusz K. Kopeć and Craig E. Banks

Received: 25 April 2023

Revised: 9 June 2023

Accepted: 12 July 2023

Published: 19 July 2023



Copyright: © 2023 by the authors. Licensee MDPI, Basel, Switzerland. This article is an open access article distributed under the terms and conditions of the Creative Commons Attribution (CC BY) license (<https://creativecommons.org/licenses/by/4.0/>).

1. Introduction

Electricity is an essential part of our everyday life. Moreover, the energy demands are ever-rising. To fulfill these demands in an eco-friendly manner, the scientific community is looking towards photovoltaic technology as the best alternative. Hence, the research on solar cells (SCs) has attained tremendous momentum for sustainable human development [1]. On the other hand, graphene and graphene derivatives have also grabbed huge researchers' interest in the past few decades. This owes to its extraordinary properties, which make it one of the most promising candidates for optic, electronic and energy-harvesting devices [2].

Graphene was first discovered by Geim and coworkers in 2004 [3]. It offers appreciably high electrical mobility (conductivity), ultrahigh optical transparency, outstanding mechanical hardness, thermal stability properties and chemical inertness [2,4]. Moreover, these properties can even be tuned as per the requirement by implementing different chemical functionalization protocols. Graphene has a special gapless band structure that exhibits an almost linear dispersion (energy-momentum) relationship at Dirac point positions in reciprocal lattice space (Brillouin zone) which is in the vicinity of the Fermi energy. The conduction and valence band edges intersect each other at the Dirac point.

This creates a continuum for charge transport and charges start behaving as massless particles [5]. This aspect of graphene can be explained by the Dirac equation for massless particles [6] and is represented using Figure 1. Thus, graphene is known as a zero band gap semiconductor or semimetal [7].

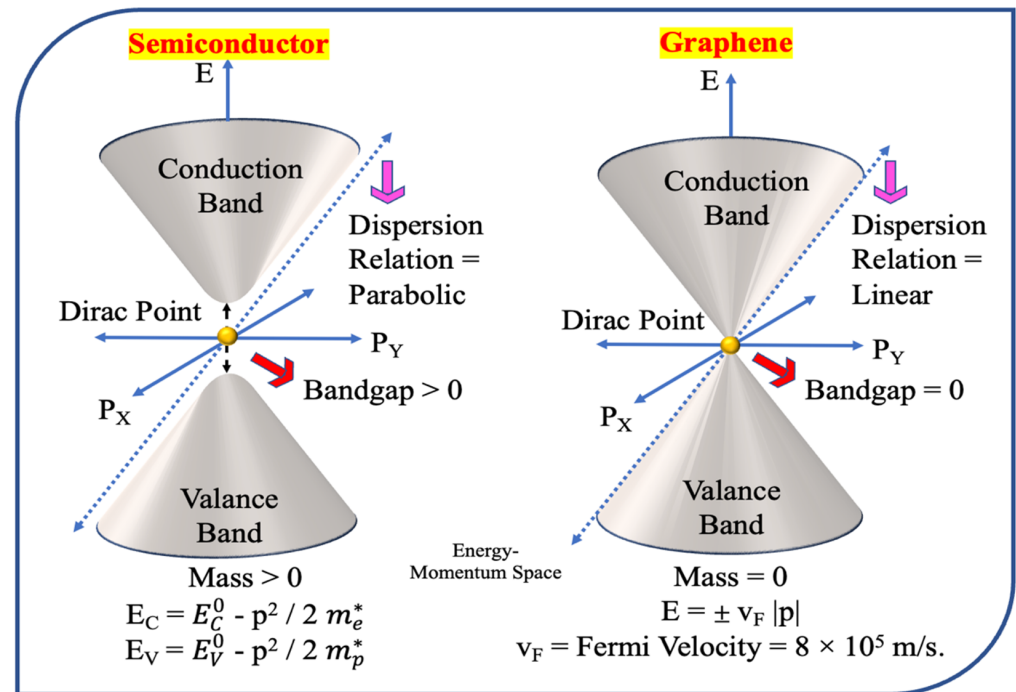


Figure 1. Three-dimensional band structure of semiconductor and graphene materials.

Figure 1 demonstrates that as a semiconductor has a finite band gap and parabolic dispersion relation, the carriers are quite massive. Thus, carriers in the conduction band possess energy, $E_C = E_C^0 - \frac{p^2}{2m_e^*}$, and carriers in the valence band possess energy, $E_V = E_V^0 - \frac{p^2}{2m_p^*}$. Here, m_e^* , m_p^* , p , E_C^0 , E_V^0 , E_C and E_V denote rest masses of electron and proton, momentum, rest mass energies and total energies of conduction band and valence band carriers, respectively. As the particles in graphene are massless, its energy is calculated similarly to that of photons (rest mass = 0). Thus, both the electrons and holes possess energy $E = \pm v_{Fermi} |p|$, where v_{Fermi} is Fermi velocity, i.e., the velocity of fastest moving charge carriers having kinetic energy equal to Fermi energy, or the velocity of charge carriers in highest occupied states at zero absolute temperature and zero external electric fields. As graphene has linear dispersion relation, the carrier group velocity/Fermi velocity is constant over energy. Thus, the carriers' effective mass in graphene is directly related to momentum and has zero value at the zero energy point (Dirac point). The high Fermi velocity of carriers in graphene ($v_{Fermi} = 8 \times 10^5 \text{ m/s}$) indicates its high conductivity property. This carrier energy difference in semiconductors and graphene better explains the exceptional carrier mobility of graphene [7]. Furthermore, it has ambipolar electrical properties, thereby enabling it to serve as a cathode as well as an anode [8,9]. This further widens its scope of applications [2].

Owing to its large conductivity and ultrahigh flat transmittivity (~97.7%) throughout the entire solar spectrum from the ultraviolet (UV) region to the infrared (IR) region (200–1100 nm), graphene is readily applied as the transparent conducting electrodes (TCEs) in energy-harvesting devices, photo-detectors and other optical devices [2,10]. Similarly, it possesses unusual electronic properties that follow Landau level quantization, quantum Hall effect, 2D Dirac fermion characteristics, etc. Thus, its free charges can easily move in two dimensions with carrier mobility of $10^6 \text{ cm}^2/\text{Vs}$ [2].

The Landau level quantization of graphene and corresponding density of states (DOS) in its Landau quantized levels is illustrated in Figure 2. It demonstrates that the allowed energy levels of graphene are discrete (not continuous). Moreover, the distance between consecutive Landau levels decreases at higher energies and is inversely proportional to the energy level quantum number (n). The magnitude of DOS remains constant at every Landau energy level. Graphene exhibits the special property of carrier multiplication [11]. The Landau quantization allows us to tune graphene's band gap and greatly benefits the carrier multiplication process, as shown by Wendler et al. [11]. This has the potential to further enhance the PCE of SC devices to a higher level.

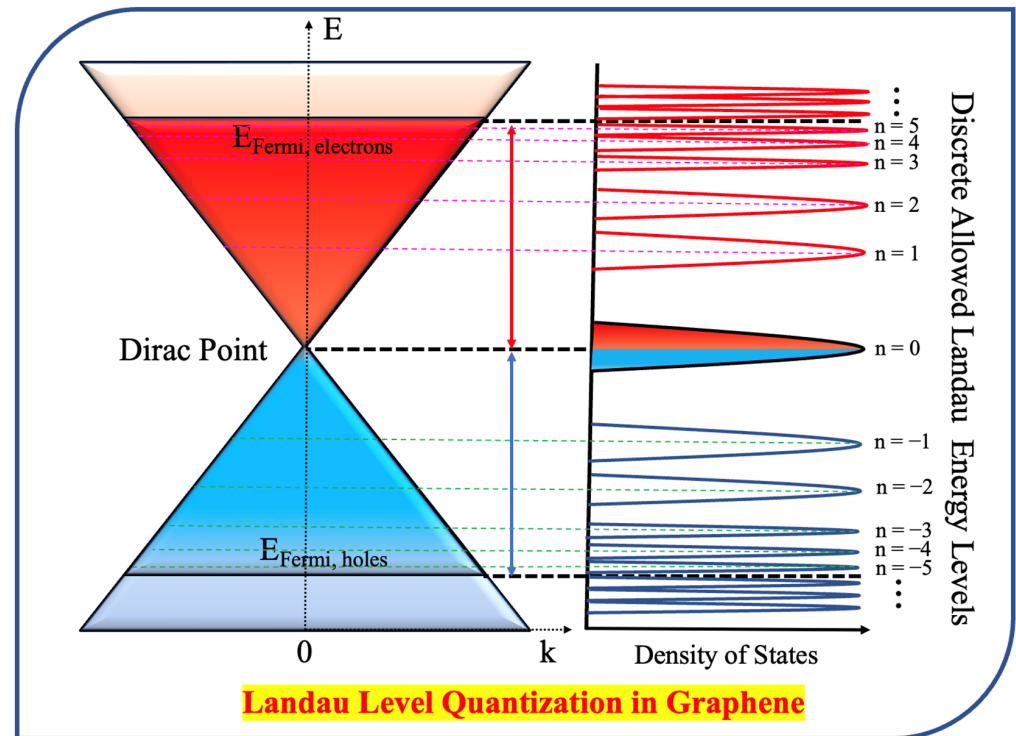


Figure 2. Landau level quantization and DOS of Landau levels in graphene.

Also, its thermal conductivity ranges between 3000 and 5000 W/mK, it has a Young's modulus of 1.1 TPa and an excellent specific surface area of 2630 m²/g tends it to exhibit excellent mechanical plus thermal properties and making it a strong candidate for flexible optoelectronics [12–14]. Its thickness-dependent semiconductor properties make it suitable for Schottky junction formation with particular metals [15]. These properties further expand its scope to advanced field-effect transistors [4], liquid crystal devices [16], Li ion battery electrodes [17–20], ultra-capacitors for low-cost high-yield energy storage [21–27], catalysts and proton-exchange membranes in fuel cells [28–31], field electron emitters [32,33], ultra-tough paper [34], organic memory devices [35], resonators [36], gas molecule detection [37], photo-detectors [38] and thermal management [39]. Hence, in a nutshell, it has found wide applications in the fields of photonics, electronics, spintronics, energy storage and conversion, durable flexible thin display screens, biomedical devices and emerging technology of graphene-based smart materials [40–49]. In this article, a rigorous review of applications of graphene for advancement in solar photovoltaic technology is presented. The graphene functional layer is shown to realize various types of highly efficient, light-weight, flexible and cost-friendly SCs in this paper.

The thickness of graphene depends on the number of layers stacked one over the other. Based on this number, graphene's structures are termed as mono-layer, bi-layer, tri-layer or multi-layered graphene which vary greatly in their characteristics [50]. Multi-layered graphene grown on flat resistive surfaces has two main advantages. Firstly, it reduces

electronic scattering thereby, decreasing sheet resistance up to 350 Ω/cm . And secondly, it increases photon scattering at surface wrinkles thereby, decreasing effective reflectance [51].

However, the disadvantage of the thick layer (~ 4 layers) is that there is a decrement in layer transmittivity to 93% in the visible and IR range [52,53]. Hence, to achieve both the desired properties of reduced sheet resistance and high transmittivity, the bi-layer (and occasionally tri-layer or 4–7 layers, depending on the SC structure) graphene becomes the most suitable and promising material for optoelectronic SC devices.

The four main advantages that graphene offers to high-tech SCs are (1.) transparent window for effective absorption and collection of incident photons; (2.) appreciable charge transport kinetics for effective photogenerated charge collection; (3.) offering flexibility to SCs along with a robust architecture; and (4.) provision of higher efficiency heat dissipation [2]. Moreover, graphene's electrocatalytic activities contribute to enhancing the performance of electrochemical SCs such as dye-sensitized solar cells (DSSCs) where the electron transport pathway is a solid/liquid interface [2]. Many more diverse applications representing the versatility of graphene in SC technology, as shown in Figure 3, are presented henceforth in this paper.

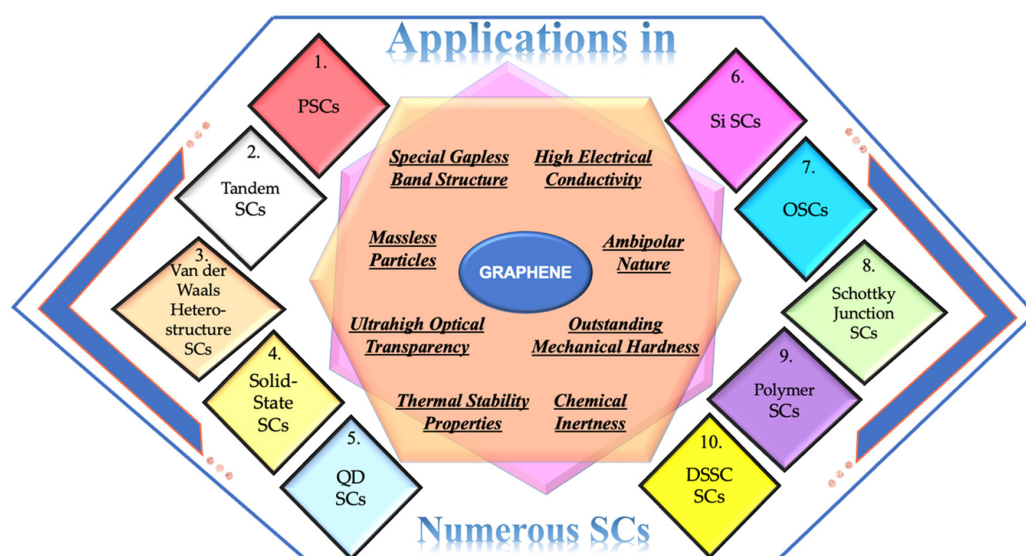


Figure 3. Schematic diagram of attractive properties and versatile applications of graphene in different SC structures reviewed in this article.

2. Methodology: Graphene Synthesis Techniques and Graphene Transfer

There are two main techniques of graphene fabrication: (1.) physical techniques that include: (a.) micro-mechanical exfoliation of highly ordered pyrolytic graphite (HOPG) [3] and (b.) sublimation at high temperatures [54]; and (2.) chemical techniques that include: (c.) graphene oxide reduction [55] and (d.) chemical vapor deposition (CVD) on metal substrates [56]. This section presents a brief overview of all major popular graphene synthesis processes. The most preferred among all synthesis techniques are the exfoliation, thermal CVD, chemical synthesis and epitaxial growth methods [2].

In the context of graphene synthesis, the major challenge is in the production of large-scale high-quality graphene at a low cost. To address this issue, scientists Shi et al. proposed non-electrified electrochemical exfoliation method [57], Li et al. proposed salt and water co-assisted exfoliation of graphite in organic solvent [58], Islam et al. presented a protocol for ultrafast chemical-free graphite exfoliation [59], Shi et al. focused on bubble-mediated mass production [60], whereas Qiao et al. proposed use of CH_4 as carbon source [61]. Owing to graphene's vast applications, its large-scale high-quality low-cost production is one of the most researched topics nowadays.

2.1. Mechanical Exfoliation

Mechanical exfoliation is a top-down approach where a single layer or a few layers of material are stripped off from bulk material by applying transverse or longitudinal stress on its surface using a simple scotch tape or atomic force microscopy (AFM) tip. This was the first experimental technique designed for few-layer graphene synthesis in the year 1999 [2]. Later on, Novoselov et al. invented a special kind of mechanical exfoliation that even successfully generated a single-atom-thick graphene structure [3]. This technique promises high-quality graphene having charge mobility of 3000–10,000 cm²/Vs [62]. Hence, mechanical exfoliation is still regarded as the best graphene fabrication technique.

2.2. Chemical Exfoliation

Chemical exfoliation is the process of intercalating and dispersing bulk graphite solution to separate out individual graphene layers. This is performed using alkali metals because they easily interact with graphite to catalyze intercalation and can form structures with different stoichiometric ratios of graphite to alkali metal. Moreover, as the atomic radii of alkali metals are smaller than the graphene interlayer distance, they are made to fit in the graphite interlayer spacing and separate off graphene layers [63,64].

2.3. Chemical Synthesis and Functionalizations

This method aims at chemically increasing the interlayer distance of pristine graphite for effective layer separation. To achieve this, graphite is oxidized to graphene oxide (GO). In this regard, the interlayer separation increases proportionally to the degree of oxidation. This oxidized graphene now facilitates graphene dispersion in suitable polar liquid solvents. Subsequently, the dispersed GO is reduced back to graphene. The quality of graphene depends on the homogeneity of GO dispersion. The advantage of this technique is that it is a low-temperature, solution-based process offering flexibility in direct graphene growth on various substrates. Moreover, graphene's catalytic and chemical properties can be easily tuned by in situ functionalization. However, the shortcoming of this method is less and defective graphene yield is often caused by incomplete reduction of graphene [2].

2.4. Thermal CVD Process

In this process, graphene is made to deposit on the surface of transition metal substrates like Ni, Cu, Pd, Pt, Ir, Ru, Fe, Co, etc. [65]. This is performed through a surface catalysis process made to occur in high-temperature CVD of hydrocarbon gases at reduced atmospheric conditions. Here, methane (CH₄) is decomposed to graphene as per the reaction: $\text{CH}_4 + \text{H}_2 \rightarrow \text{C} + 2\text{H}_2$. As it is a catalyzing process, there is no limitation on the substrate size, thereby making CVD a scalable process. However, procurement of large-scale homogeneous graphene is challenged by the formation of ripples and grain boundaries in graphene that cause defects. These defects further result in charge scattering and degrade graphene's thermal, electrical and optical properties [2]. Thus, this method is incorporated only for research purposes.

2.5. Epitaxial Growth

Epitaxial growth is employed whenever there is requirement of highly-crystalline, high-quality, superior-grade epitaxial graphene having few grain boundaries and large domain size. This is achieved using the Si sublimation technique on a well-prepared and cleaned single crystalline SiC substrate. Surface preparation is performed using oxidation or H₂ etching. Surface cleaning is performed by bombarding high-energy electrons to create 10¹⁰ Torr pressure under 1250–1450 °C temperature for 1–20 min. This high-temperature process creates anisotropy in graphene [66–68]. The drawback of this technique is that the graphene transfer from SiC to other substrates is quite hard. Secondly, the process is too expensive. This seriously restricts its application for commercial SC production.

2.6. Graphene Transfer

Graphene is synthesized using the above-mentioned popular methods. For each synthesis method, it needs to follow specifications regarding the substrate material. Hence, to obtain graphene on a desired substrate, the synthesized graphene in dispersion solution, metal foil or thin film is transferred to the desired substrate such as glass or a flexible material after final synthesis. Popular methods of graphene transfer from dispersed solution to a substrate are spin coating [52,69], drop-casting, dip casting [52,70] and electrophoretic deposition [71]. To transfer graphene to a transparent flexible substrate, methods like spraying [72], vacuum filtration [73], self-assembly methods [74–77] and Langmuir–Blodgett assembly [78] are incorporated. If graphene is in the form of metal foils, it is transferred using the PDMS transfer process [79], chemical transfer process [80,81], stamping process [82], hot press lamination process [83], and roll-to-roll transfer process [84].

However, the major challenge concerning graphene transfer is its integration into the SC architecture without compromising its properties. Thus, in order to conduct proper integration, experimentalists ensure the maintenance of proper working conditions while making contact between graphene and semiconductor [85–88].

3. Impact of Graphene on SC Technology

To effectively utilize graphene's remarkable properties for enhancing SC efficiency, one needs to have a clear idea about graphene's controllable parameters and the exact physics behind its internal mechanism. This section presents an intensive review of graphene's two controllable parameters namely, its number of layers and doping, along with their physical working to achieve high SC efficiency. Moreover, the different roles that graphene can play in SC technology like behaving as an efficient TCE, photoactive layer and Schottky junction are presented in detail. Finally, the application of graphene in 10 different types of SC technology is put forth in this section. It also includes multiple ways in which graphene can be utilized to flourish the same type of SC technology. Hence, an exhaustive review of all the researched approaches for the effective usage of graphene in photovoltaic technology is presented henceforth.

3.1. Controllable Graphene Parameters for High Efficiency of SCs

There are myriad allotropes of carbon available to us. But there are only a few specific allotropes that can be successfully implemented into SCs. The aspect that made such allotropes unique as compared to the rest of the allotropes is their ability to tune electronic, optical and thermal properties. Graphene allows its properties to be easily tuned and improved depending on its layer thickness and doping concentration. Hence, these are the two special standout parameters that optimize graphene's performance and make graphene suitable for SC applications. The following discussion mentions how exactly the number of graphene layers and graphene doping concentration impact SC efficiency.

3.1.1. Impact of Graphene Layer Thickness on SC Efficiency

Wang et al. experimentally demonstrated a proportional decrease in optical transparency (transmittance) with an increase in layer number from 1 to 8 [89]. This is even demonstrated graphically in various research works [89,90]. Researchers also noted the decrease in series and sheet resistance of graphene structure with graphene's rising number of layers [89,91,92]. However, although the nature of variation remains the same, the exact amount of reduction in transmittance, variation in sheet resistance, series resistance, shunt resistance, work function, open-circuit voltage (V_{oc}), short-circuit current (J_{sc}), fill factor and efficiency with graphene thickness is purely subjective to the consecutive layers of graphene layer, dopant type, doping concentrations and the SC structure entirely [2,9,90,93,94]. This is demonstrated in great detail by Singh et al. [93].

In the case of Lui et al., they tried 1–4 graphene layers in Ag/P₃HT:PCBM/PEDOT:PSS+Au/graphene and obtained maximum efficiency for bi-layer graphene [93]. Usually the bi-layer and tri-layer graphene results in maximum SC efficiency. This is basically

due to the fact that the bi-layer and tri-layer graphene establishes a balance between its transparency and sheet resistance properties. However, there are a few exceptions to it.

As the transparency, as well as the sheet resistance of graphene structure, always reduces with the number of graphene layers, Figure 4 demonstrates the general nature of variation in transparency (%) and sheet conductance $(\Omega/\text{sq})^{-1}$ (reciprocal of sheet resistance) with the number of graphene layers. This nature of graphs is in line with experimental graphs presented by Li et al. and Singh et al. [90,93]. From Figure 4, it can be inferred that usually the mono-layer, four-layer and multi-layer graphene may produce less SC efficiency owing to less sheet conductance in the case of mono-layer graphene and less transparency in the case of four-layer and multi-layer graphene. Thus, bi-layer and tri-layer graphene, in most cases, offer high efficiency attributed to their adequate transparency as well as sheet conductance [2,9,90,93,94]. However, the variation in sheet conductance, and thereby the exact choice of the number of graphene layers depends on SC structure entirely.

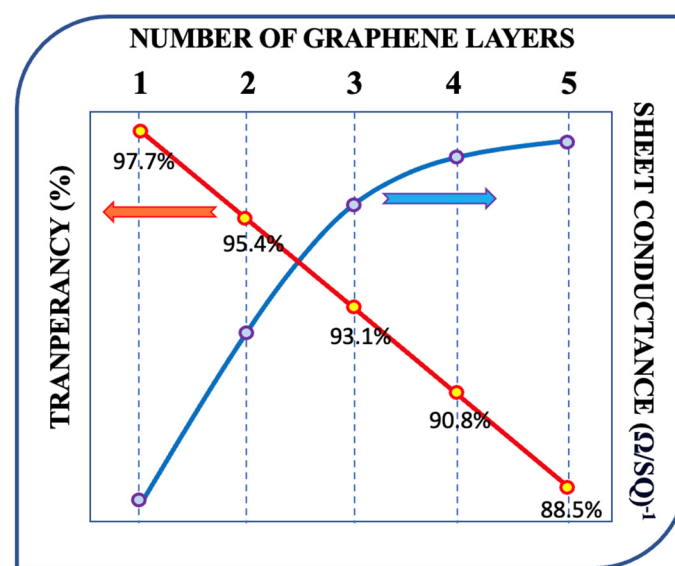


Figure 4. Variation of transparency and sheet conductance as a function of the number of graphene layers.

The sheet resistance (Ω/sq) can be theoretically obtained using the formula $R_{sheet} = \rho/t$, where ρ is the electrical resistivity and t is layer thickness [95]. However, Liu et al. demonstrated that the sheet resistance varies depending on the graphene synthesis process and type of dopant [96]. Li et al. [90], Singh et al. [93] and Wei et al. [97] provide a graphical representation of an increase in sheet resistance and a reduction in sheet conductance with number of graphene layers. From these graphs, one can interpret that the sheet resistance of graphene-based SCs is also dependent on various aspects like SC structure, graphene synthesis and deposition process, SC working conditions, etc. This is the main reason behind the qualitative nature of the sheet conductance graph with respect to the number of graphene layers in Figure 4.

Based on sheet resistance and optical transmittance, the SC efficiency is decided. For maximum SC efficiency, the sheet resistance should be small and optical transmittance should be large. With an increase in the number of graphene layers, both the optical transmittance and sheet resistance decrease (sheet conductance increases). Thus, sheet resistance and optical transmittance are two competing parameters for high efficiency of graphene-based SCs.

As the values of sheet resistance and optical transmittance depend on SC structure, we obtain the highest efficiency at different numbers of graphene layers for different SCs. The number of graphene layers providing maximum SC efficiency is seven layers in the case of Ishikawa et al. [98], five layers in the case of Notte et al. [99] and one layer in the case of Arefinia et al. [100]. However, bi-layer and tri-layer graphene, in most cases, offer

high efficiency attributed to their adequate transparency as well as sheet conductance as seen in the research studies of many scientists [2,9,90,93,94].

In this context, precisely controlling graphene's number of layers is a quite challenging task. To address this issue, i.e., to achieve controllable growth of graphene, Cho et al. established control over the growth pressure [101], Lin et al. adopted a pico-second laser thinning technique [102] and Tu et al. and Negishi et al. performed controlled CVD [103,104]. Sun et al. demonstrated fine control over graphene's number of layers by adjusting the amount of intercalated carbon source [105] whereas, Wang et al. achieved the same task by implementing ultrasound in super-critical CO₂ [106].

3.1.2. Impact of Graphene Doping on SC Efficiency

Graphene's doping profile including doping concentration and dopant type largely influences graphene's physical, optical and chemical properties [107]. Wang et al. deeply studied the effect of heteroatom doping on graphene's electrical and electrochemical properties [108,109]. Singh et al. made a rigorous analysis of variation in SC efficiency with graphene's doping profile [93]. They observed that there is a decrease in series resistance, sheet resistance, mobility and transmittance and an increase in Schottky/ohmic barrier height, electrical conductivity and work function with an increase in graphene doping [93,94].

This is because there is a shift in the Fermi level position of graphene with doping as illustrated in Figure 5 [94]. Figure 5 clearly demonstrates the direction of Fermi level shifting as a function of doping type. It is situated exactly in the middle of the conduction band (CB) and valence band (VB) in the case of pristine undoped graphene. As graphene is ambipolar, it can be doped using both the n-type as well as a p-type impurity as shown by Shin et al. [94]. P-type doping of graphene shifts graphene's Fermi level towards VB and n-type doping shifts it towards CB. More doping generates a larger amount of shift in the Fermi level for the creation of larger built-in electric field/potential inside SC. It acts as a driving force for efficient charge collection. Here, E_{Fermi} is the energy associated with the Fermi level.

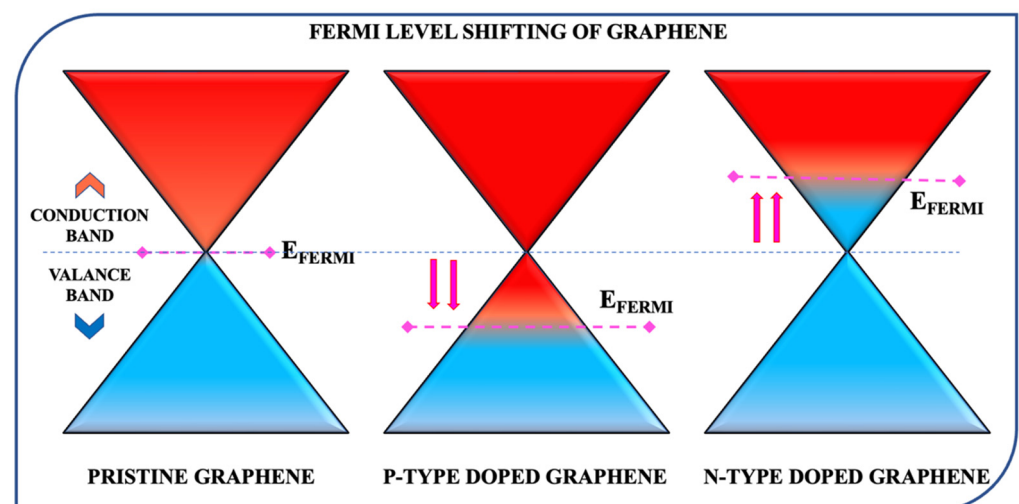


Figure 5. Schematic diagram of shift in graphene's Fermi level with respect to type of doping.

Shifting of graphene's Fermi level leads to an increase in graphene's work function in the case of p-type doping and a decrease in its work function in the case of n-type doping. However, the exact graph is subjective to the SC structure, dopant type, dopant concentration, experimental conditions, etc. The exact nature of the graphs can be inferred from the studies conducted by Shin et al. [94], Yang et al. [110], Kwon et al. [111], Shi et al. [112] and Garg et al. [113].

Now, to understand precisely the effect of variation in work function on SC efficiency, Figures 6 and 7 demonstrate the variation of graphene/semiconductor band alignment as a function of graphene work function and doping. In Figure 6, graphene is chosen to be p-type doped. Hence, an increase in graphene's p-type doping increases the graphene work function. From Figure 6, one can understand that as the graphene's work function increases above the zero-energy level or vacuum level of the semiconductor, the CB and VB tend to bend upwards at the graphene/semiconductor interface. This leads to the formation of ohmic contact at the graphene/semiconductor junction. Now, as the p-type doping increases, the graphene work function increases too, thereby increasing the band bending at the graphene/semiconductor junction. More bending results in accelerated charge transfer and collection at graphene anode and semiconductor cathode terminals. Thus, the efficiency of graphene to behave as an anode in SCs is enhanced. This increases the current density and ultimately improves the graphene-based SC efficiency [94].

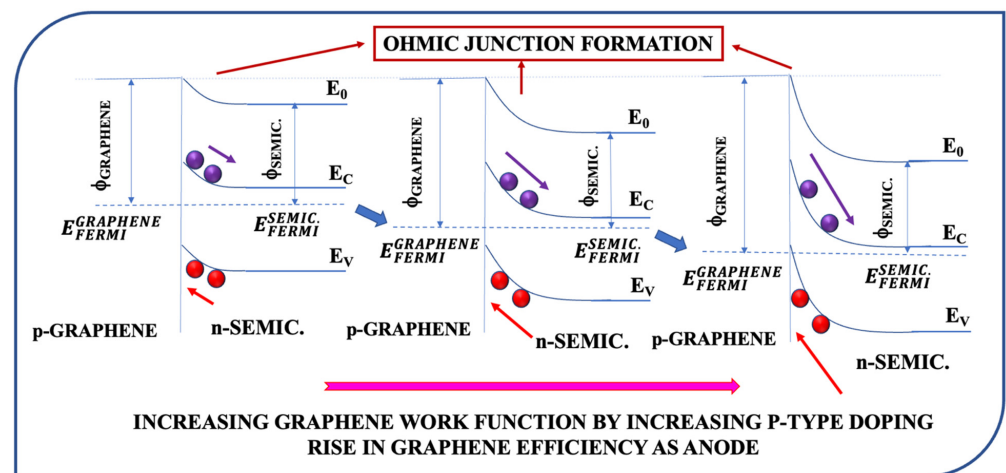


Figure 6. Variation of p-graphene/n-semiconductor junction band alignment with p-type doping.

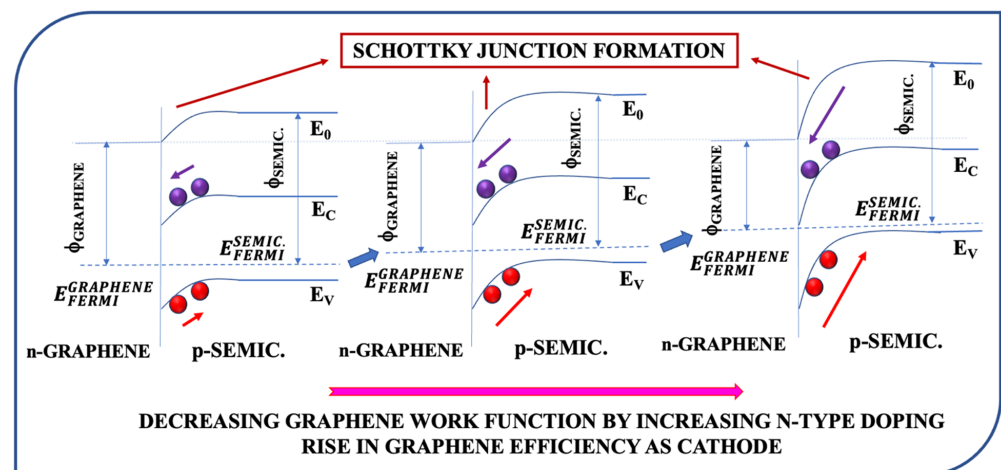


Figure 7. Variation of n-graphene/p-semiconductor junction band alignment with n-type doping.

Similarly in Figure 7, graphene is chosen to be n-type doped. Hence, an increase in graphene's n-type doping decreases the graphene work function. From Figure 7, one can again understand that as the graphene's work function decreases below the zero-energy level of the semiconductor, the CB and VB tend to bend downwards at the graphene/semiconductor interface. This time, it leads to the formation of Schottky contact at the graphene/semiconductor junction. Now, as the n-type doping increases, the graphene work function further decreases, thereby increasing the band bending at the

graphene/semiconductor junction. As mentioned earlier, more bending results in increased rapidity of charge transfer and collection at graphene cathode and semiconductor anode terminals. Thus, the efficiency of graphene to behave as a cathode in SCs is enhanced. This enhances the current density and ultimately boosts the graphene-based SC efficiency. Thus, there is a rise in SC efficiency with graphene doping [93,94]. Patel has also demonstrated that the enhancement in barrier height of ohmic and Schottky junctions led to an increase in his proposed SC efficiency [114]. Here too, the amount of increase in SC efficiency depends completely on the SC structure, dopant type and concentration.

In both Figures 6 and 7, ϕ_{GRAPHENE} , ϕ_{SEMIC} , $E_{\text{FERMI}}^{\text{GRAPHENE}}$, $E_{\text{FERMI}}^{\text{SEMIC}}$, E_0 , E_C and E_V denote the work function of graphene and semiconductor, Fermi level energy of graphene and semiconductor, zero-energy level or vacuum level energy, LUMO (CB) energy and HOMO (VB) energy of semiconductor, respectively.

Owing to the significance of proper doping of graphene, Hu et al. performed an intensive study specially dedicated to presenting the impact of optimized doping of graphene films for its wide applications in electronics and optoelectronics [115]. Precise control of graphene's doping process is quite a difficult challenge. Apart from heteroatom doping, the other types of doping can be chemical doping and electrostatic field doping. Electrostatic field doping can also be adopted to manage graphene's work function to improve Schottky barrier height [3,116–119]. The external back gate is made of atomic layer-deposited ferroelectric or dielectric polymer and is tuned by electric field/voltage. This gate can now, be utilized for graphene's electric field doping. In this doping, electrons are induced by the positive voltage, whereas, holes are induced by negative voltage, making graphene n-type or p-type doped [9].

For optimized graphene doping to achieve high-performance SCs, Liu et al. adopted Nafion doping and plasma etching and achieved 9.2% efficiency experimentally [120]. In order to provide a viable way to finely tune graphene doping for desired electronic properties, Shamim et al. recently controlled doping concentration and choice of dopant for high-capacity negative electrodes for Li and Na ion batteries [121]. Ubhi et al. analyzed phosphorous and boron-doped graphene to benefit various energy applications such as fuel and solar cells, supercapacitors and batteries [122]. Mollaamin et al. also doped graphene with various dopants such as nickel, iron and zinc during their study and observed the variation in graphene's performance [123]. Moreover, the doping can also be performed through various methods such as solid, liquid and gas phase chemical doping, thermal annealing, ball milling, CVD: in situ doping, plasma treatment, etc.

Achieving high doping concentration in graphene while simultaneously maintaining graphene's structural integrity is also a challenge. Hence, recently Kandula et al. [124], Zhang et al. [125], Kim et al. [126] and many more scientists demonstrated various ways to overcome this issue. Kandula et al. fabricated highly conductive dual-doped graphene-based nanorattles while ensuring the maintenance of their structural integrity [124]. Zhang et al. prepared nitrogen-doped graphene such that the device maintained its structural integrity up to 150 °C [125]. Also, Kim et al. showed mechanically resilient nitrogen-doped graphene that fairly maintained its structure during the doping process [126].

Often, doping graphene introduces defects and impurities in it, which can reduce its electronic mobility and degrade its performance. Doping and defects are so interrelated that doped graphene is sometimes called defective graphene [127]. To resolve this issue, He et al. presented an experimental way of ion implantation to achieve low-damage less defective phosphorous-doped graphene [128]. Also, Tung et al. engineered nitrogen-doped graphene film that offered high mobility and conductivity [129]. They achieved such high-quality doped graphene through a combination of ultrasonic spraying, microwave irradiation and thermal annealing methods. Similarly, the research of Qiu et al. also demonstrates the fabrication of high-performance highly conductive (high mobility, less defective) nitrogen-doped graphene sheets for supercapacitor applications [130].

To fully utilize the potential of doped graphene for SC efficiency enhancement, Al-Aqtash et al. and Lambin et al. followed the approach of studying microscopic in-

teractions between the dopants and graphene [131,132]. Moreover, recently, Abdullah et al. noted stacking orientation caused in bi-layer graphene due to interaction between B and N dopant atoms [133]. To develop further intricate understanding, more such studies need to be performed.

3.2. Different Roles of Graphene in PV Technology

This section presents a thorough study of various possible applications for utilizing graphene's attractive properties in SC technology.

3.2.1. Graphene Transparent Conducting Electrodes

Despite possessing high electrical conductivity and optical transparency above 90%, the previously famous metal TCEs such as indium tin oxide (ITO) and fluorine-doped tin oxide (FTO) lacked in providing flexibility to SC devices [134,135]. This is owed to the brittleness of metal TCEs. Moreover, metals even restricted the SC aperture area [136]. Furthermore, ITO contains indium which is a very scarce metal and is produced in limited amounts per year. Additionally, as the demand for TCEs rose with the development of solar photovoltaic technology, the prices of indium also rose [137,138]. Analysis reveals that it was TCE that accounted for 50% of SC manufacturing costs. This was because TCEs were synthesized by the high-temperature vacuum deposition method which is a very expensive process. This was a major challenge for the low-cost production of SCs [139]. Also, indium is toxic (not eco-friendly) in nature [2]. Hence, they were not the ideal choice as SC TCE. Therefore, finding an alternative substitution for TCEs and replacing ITO and FTO was of great importance [94].

In recent years, various TCEs like conductive polymers, carbon nanotubes (CNT) random meshes, GO, graphene, metal nanowires (NWs) films, gratings and nano-grids, etc., were tried out for SCs [5,94,140]. Among them, GO, CNT and metal NWs couldn't provide entire substrate surface area coverage [94]. Conductive polymers also had short-comings such as low solubility that limits processability, complex synthesis processes and chemical instability in an ambient environment [94]. Moreover, the conventional TCEs had further demerits like complex structure, defect and doping-caused unavoidable charge scattering centers, difficulty in controlling resistivity, etc. This limited the SC performance greatly [2].

Comparatively, the newly introduced graphene offers high transmittance throughout the entire solar spectrum (93–97% over wavelengths 400–1100 nm), better conductivity and charge mobility (10^6 cm²/Vs), good chemical stability, excellent flexibility due to outstanding mechanical and thermal properties, easy tuning of sheet resistance, Fermi level and work function by doping, low production cost, less weight, etc. Hence, it is evident that graphene outperforms ITO and other conventional TCEs due to its excellent properties [2,5,90,94]. This is the reason why graphene has become so popular as TCEs. Even the TCEs combinedly made up of graphene and PEN, PEDOT:PSS and other inorganic oxides show high efficiency and excellent mechanical strength [2].

To make graphene suitable for TCE, the value of the ratio between sheet resistance and transmittance (R_{sheet}/T) needs to be increased. To determine this ratio, the parameter under experimental evaluation is the DC conductivity vs. optical conductivity ratio (σ_{DC}/σ_{op}).

T and R_{sheet} are related to σ_{DC}/σ_{op} by the equation $T = 1 / \left[1 + \left(\frac{Z_0}{2R_{sheet}} \right) \left(\frac{\sigma_{op}}{\sigma_{DC}} \right) \right]^2$, where Z_0 is the impedance of free space [141]. Hence, higher σ_{DC}/σ_{op} indicates an efficient TCE with high T and low R_{sheet} . The minimum industry standard σ_{DC}/σ_{op} value for transparent conducting oxide (TCO) substitution is 35 [142,143].

3.2.2. Graphene Photoactive Layers

The photoactive layers in photovoltaic devices include active interfacial layers, the electron/hole charge separation layers, the electron/hole transport layers (ETL/HTL) [93], the electron/hole charge blocking layers [144] and the buffer layer [145]. Owing to its properties, graphene acts as an efficient photoactive layer playing diverse roles in SCs. Graphene and its derivatives have also demonstrated a reduction in exciton decay, a

decrease in interfacial recombination and leakage current and an increase in shunt resistance when it was applied as a photoactive layer by Uma et al. [146], Zhang et al. [147], Li et al. [148] and Liu et al. [149]. This consequently improved the experimental efficiency of their respective SCs. Being ambipolar in nature, graphene also offers good rectification characteristics and facilitates electron/hole blocking. Hence, it behaves as an anode as well as a cathode layer [150–153].

Apart from graphene, many other graphene hybrid materials are adopted as photoactive layers. Kakavelakis et al. employed lithium-neutralized graphene oxide (GO-Li) as an interfacial layer [154]. They too obtained efficiency upliftment from 5.51% without GO-Li to 6.29% with GO-Li photoactive layer in their SC. Along with SC efficiency, it also improved the SC stability against solar heat, air and moisture. Increasing the layer thickness further increased the SC performance. It can also be used as an antireflective protecting film due to its chemical inertness and high transparency. Singh et al. provide a lot of technical details to present this aspect of graphene in their article [93]. This role of graphene is projected in various SCs and is discussed in detail in the following Section 3.3.

The other notable graphene-based photoactive layers include thiolate-reduced graphene oxide (TrGO) material producing an efficiency of 4.20%, graphene-C₆₀-silver-based hybrid material exhibiting an efficiency of 7.2%, graphene and transition metal oxide composite with an efficiency of 7.3%, graphene-CdS-based materials offering efficiency of 7.5%, etc. [93].

3.2.3. Graphene Schottky Junctions

As pristine graphene has zero band gap, the Schottky junction barrier formed using graphene has a purely metallic nature. It can be attained by simple work function tuning. The metallic nature is explained by the doped atoms that become very close neighbors of each other and they form a continuous band of charge carriers. Thus, the recombination sites get removed. This increases the SC efficiency [9]. Moreover, graphene's high transparency allows a large amount of sunlight to pass through it and is absorbed by SC. Hence, a large number of photogenerated electron-hole pairs are generated [9]. Here, a large electric field/built-in potential and space charge region is produced at the Schottky junction due to the work function difference in graphene and its consecutive layer [9,94]. This readily separates and extracts the electron-hole pair for their effective collection via the Schottky junction [9]. This is a direct consequence of suppression in reverse saturation current causing a reduction in recombination processes at these junction interfaces.

Work function is the most influential parameter that determines the nature of the junction. As discussed in Section 3.1.2, graphene allows its work function to be easily tuned by controlling the graphene doping profile. Being ambipolar, graphene can be doped by both n-type and p-type doping. Analyzing deeply, p-type impurities drive the graphene Fermi level above the Dirac point, whereas, n-type impurities drive it below the Dirac point [151,155–158]. This is pictorially explained by Das et al. in their study [9]. This allows tuning of graphene's work function, reduces sheet resistance and facilitates efficient charge extraction. This effect of Schottky junction formation is schematically explained in detail in Section 3.1.2.

3.3. Application of Graphene in Various Types of SCs

This section describes advancements in 10 different types of SC technologies caused due to incorporation of graphene and its derivatives in the SC structure. The graphene-based SCs are observed to outperform those SCs with the same configuration but lacking the presence of graphene in them. The various roles that graphene efficiently performs in individual types of SC technology are also explored.

3.3.1. Application of Graphene in Silicon SCs: The Graphene/Si SCs

The first-generation silicon SCs are still the most popular commercial SC devices owing to their appreciably high efficiencies. This is due to their extremely high optical absorption coefficient over the entire wide range of the solar spectrum from the ultraviolet

(UV) to the near-infrared (near-IR) wavelength region. Moreover, Si is an eco-friendly non-toxic material. Si-based SC manufacturing process is also simple. This makes it an excellent material for efficient sunlight harvesting.

After graphene's discovery in 2004, graphene was first used as TCE in Si-SCs in 2010 [159]. But, the high sheet resistance of graphene resulted in low SC efficiency of just 1.7%. Since then, there has been a lot of research on graphene TCE-based Si SC. Now, graphene has been used as TCE as well as various junctions in graphene/Si SCs, namely, n-type heterojunctions, p-type heterojunctions and Schottky junctions. Zero band gap graphene creates a Schottky junction with Si [9,160]. It is schematically shown by Shin et al. [94].

The work function difference creates a space charge region and built-in potential that easily extracts charge carriers in graphene/Si SCs. The energy band diagram of graphene/Si SC is illustrated by Das et al. [9]. The band bending is seen to be upwards in the case of p-graphene/n-Si SC and downwards in the case of n-graphene/p-Si SC as shown in Figures 4 and 5 [161].

The efficiency of graphene/Si SCs is still below 10% [94]. Among different graphene hybrid doped derivatives, solution-treated Ag NWs offer maximum SC performance [162,163]. Moreover, Ag NWs/graphene hybrid TCEs resulted in high efficiency of 8.68% [164]. The HNO₃-Au NP co-doped graphene TCE in Si SC achieved high work function and conductivity to yield SC efficiency of 10.20% [165,166]. These results conclude that the efficiency can be enhanced by co-doping instead of single-atom-type doping. This result was reconfirmed by obtaining high efficiency of graphene/Si SC due to Ag NW-AuCl₃ co-doping [167]. Thus, graphene's high transmittance and efficient charge carrier collection due to Schottky barrier formation benefit graphene/Si SCs to achieve higher efficiencies [9]. Das et al. provide further detailed analysis of the role of graphene as TCE and as a junction layer in graphene/Si SCs [9]. The application of graphene in different Si SCs is discussed below.

Application of Graphene in Porous Silicon SC: Graphene/PSi SC

Porous Si (PSi) is a promising material that offers inherent antireflection effects along with additional advantages of broad optical absorption, band gap widening and effective surface passivation/texturization [168,169]. Moreover, its antireflection effects can be enhanced by controlling its porosity leading to a large surface-to-volume ratio [170]. Hence, to know the effect of graphene in such SCs, the graphene/PSi Schottky junction SCs were recently studied by various scientists. It is diagrammatically represented by Shin et al. [94]. Despite doping graphene, the resulting efficiency of graphene/PSi was relatively low about 4.3% [171].

As a solution, its efficiency was enhanced by employing multi-layer graphene TCEs. The optimum number of graphene layers was set, as well as the multi-layer graphene was doped with various kinds of metal chlorides [172]. Among them, the RhCl₃-doped bi-layer graphene/PSi yielded the best performance with an efficiency of 9.15%. It also possessed good stability by retaining about 80% efficiency even after 10 days in air. This is schematically demonstrated by Shin et al. [94]. Furthermore, very recently, graphene TCEs co-doped with p-type dopants Au NPs and bis-(trifluoromethanesulfonyl) amide (TFSA) enhanced graphene/Psi SC efficiency up to 10.69% using 9 mm² active area [173].

Application of Graphene in Silicon Nanowires SCs: Graphene/Si NWs SC

Si NWs-based SCs are also considered promising SC types for sunlight harvesting owing to their nanostructure-facilitated fast electronic transport and low reflectance as compared to thin films over a broad solar spectrum. This is pictorially demonstrated by Shin et al. [94,174,175]. Hence, Si NWs-based SCs have a large interface area for light trapping. Thus, such SCs can work efficiently even without explicitly depositing antireflective coatings.

Hence, the research on Si NWs-based SCs using graphene TCEs has been recently increasing. HNO₃-doped graphene/Si NWs SC has been shown to offer an efficiency of about 6.85% [147]. Although the efficiency was quite less, the results indicate that the efficiency of graphene/Si NWs SCs can be further increased by continuous research efforts [140].

Application of Graphene in Silicon Quantum Dot SCs: Graphene/Si QD SC

Employing Si quantum dots (SQDs) is a thoughtful solution to overcome the shortcoming of Si regarding its small indirect band gap nature, thereby making it more efficient as a photovoltaic device [176,177]. Controlling SQD size allows tuning its band gap due to the quantum confinement effect. Proper band alignment increases the efficiency of SCs according to the band offset optimization proposed by Minemoto et al. [178] and the concept of band offset uniqueness proposed in my previous paper [179]. Earlier designed metal TCE-based metal TCE/SQD SCs offered efficiency in the range of 10.4–14.8% [180–184]. A recent study on the utilization of graphene TCEs in graphene/SQDs:SiO₂/Si heterojunction SC showed maximum efficiency of 16.2% [167]. This was much larger compared to the ever-reported efficiency of metal TCE/SQD SCs. This result is schematically illustrated by Shin and coworkers [94].

Here, the graphene/SQD SC performance depends on diode quality, energy barrier at the graphene TCE/SQD interface, doping-dependent T/R_{sheet} value of graphene and graphene thickness-dependent reflectance value [94,185]. For efficient charge transport and collection in SQD SCs, graphene TCEs are doped with two kinds of dopants namely, Ag NWs and AuCl₃. Here, the doped-graphene TCE must be protected/encapsulated using another graphene layer to prevent dopants from oxidizing/destroying and the efficiency of SCs is further increased. The impact of graphene/SQD SC doping on increasing SC efficiency and long-term SC stability is graphically shown by Shin et al. [94].

3.3.2. Application of Graphene in Polymer SC: Graphene/Polymer SC

The polymer-based SCs are valuable SC types in the photovoltaic industry because their properties can easily be tailored as per the requirement. They offer many advantages over inorganic-material-based SCs. They can easily be deposited using solution-based processing techniques on ultrathin films. The material is also inexpensive, making large-scale SC production possible [93]. In the last few decades, polymer SCs have found promising applications in bulk heterojunction (BHJ) devices [186]. Scientists developed elastic [187–189] as well as rigid [190] BHJ polymer SCs, and devices in inverted [191–193] as well as in direct [193] configurations. Moreover, tandem polymer BHJ SCs were also explored [194,195]. Iwan et al. have presented a rigorous study on the use of graphene in polymer-based SCs [196]. In such SCs, graphene can play three roles: (1.) as an additive in donor or donor–acceptor materials, (2.) as TCE, i.e., anode and cathode and (3.) as a separate photoactive layer. They have experimentally tabulated and demonstrated that graphene increases the efficiency of polymer-based SCs.

Here, the graphene facilitates effective charge separation when mixed with the conjugated polymers [87]. Graphene provides a continuous pathway with multiple donor/acceptor sites due to its large surface area. This allows efficient charge transfer. But the efficiency of graphene/polymer SCs is quite low.

Graphene, when mixed with polymeric materials, produces a material with different band gap. This material employed as HTL may stop leakage current and prevent charge recombination while prohibiting electron migration from cathode to anode.

3.3.3. Application of Graphene in Schottky Junction Solar Cells: Graphene/Schottky Junction SC

Physically, any material can form a Schottky junction with a certain material provided that the difference in their work function is large enough [197]. Thus, materials that can form Schottky junctions with graphene are GaAs, Si, GaN, GO, SiC, CdS, CdSe, etc. [198–205]. Intensive research has improved the efficiency of graphene/Si Schottky junction SCs up to 14.5% [88,206].

As GaAs provides a direct band gap and higher mobility as compared to Si, the research on the impact of introducing graphene in GaAs-based SCs was initiated. The simulations predicted superior performance of graphene/GaAs heterojunction SC as compared to graphene/Si junction [15]. Experimentally and through formulations, Jei et al. made efforts

to prove this fact [206]. The rectifying behavior was determined by calculating Schottky barrier height, series resistance, energy band diagram, built-in potential, charge separation and extraction, etc., for single and bi-layer graphene. Their results suggested that the bi-layer graphene exhibits higher Schottky barrier height (0.75 eV), smaller ideality factor (2.43) and lower series resistance (20.1 Ω) as compared to mono-layer graphene. Hence, bi-layer graphene/GaAs Schottky junction SC performs better than mono-layer graphene [206].

Tongay et al. demonstrated enhanced efficiency of graphene/nSi Schottky junction SC up to 8%. They also illustrated experimentally that the TFSA dopant enhanced SC stability due to its hydrophobic nature [199]. As graphene's properties are tunable, it can be used to optimize SC as well as can be applied to diverse materials. Moreover, graphene electrodes are less costly and can easily be fabricated. Hence, graphene is considered to have the potential to easily outperform ITO to form Schottky junction SCs [207].

3.3.4. Application of Graphene in Dye-Sensitized SC: Graphene-Based DSSCs

Over the last few years, DSSCs have become known for their unique characteristics such as rapid electron transport, tunable electrochemical properties and outstanding light transmittance capability [81,208–211]. The third generation of DSSCs is looked upon as the promising SC technology due to rapid photo-charge generation, utilization of non-toxic elements and low-cost production. Graphene has recently been integrated with DSSCs to enhance its efficiency [212]. In these SCs, graphene is made to act as (1.) photoanodes, (2.) counter electrodes, (3.) sensitizers and (4.) photoanode additives. The various aspects and underlying physics behind the applications of graphene are discussed henceforth.

Application of Graphene as Photoanode in DSSCs

As graphene has a large transmittance value of ~97%, Wang et al. made an attempt to utilize graphene as a photoanode in DSSCs. Thus, they laid a new pathway for research on graphene-based DSSCs [70]. Photoanode in DSSCs is an electron vehicle that is responsible for carrying photogenerated electrons from the excited dye sensitizers to the outer circuitry. In this case, graphene can fit as a promising photoanode with TiO₂ dye, attributed to its excellent conductivity and mobility properties [213–215]. Along with being spatially well dispersed, graphene also facilitates the making of crack-free TiO₂ mesoporous thick films [216]. Hence, graphene extends high feasibility with TiO₂ nanocrystalline particles [217].

Experiments have observed enhancement in J_{sc} in graphene-based DSSC as compared to bare TiO₂ electrodes [218]. This enhancement in J_{sc} is attributed to the optical scattering effect. It leads to enhanced red photon harvesting and easy charge transport through TiO₂/dye interface via graphene expressway. This promotes efficient charge collection at photoanode [219]. Here, the graphene composite quantity in wt% directly influences SC efficiency. More graphene can reduce its transparency in the TiO₂ matrix as well as decrease the dye-loading amount. Hence, instead of conventional 2D composite electrodes, the three-dimensional (3D) wide-pore graphene structure started to be used [220,221]. This appreciably improved the performance merit of graphene-based DSSCs by increasing energy transfer sites and reducing the recombination rate at TiO₂/dye interface [94].

Moreover, as discussed earlier, graphene has the potential to replace ITO and FTO as TCE. The same is the case seen in DSSCs as well. Compared to ITO and FTO, graphene acts as a better TCE photoanode in DSSCs, offering it stretchability, bendability, flexibility, high transparency and conductivity, surface uniformity, thermal stability and cost balancing [91,222].

Application of Graphene as Counter Electrode Material in DSSCs

In DSSCs, counter electrodes play an essential role in injecting electrons from photo-oxidized dye into electrolytes for catalyzing reduction reactions. This reaction determines current generation and dye regeneration [223–228]. Platinum (Pt) was widely used for this purpose owing to its low resistance and incredible catalytic activity. But, due to its high cost, limited abundance and chemical inertness, it has become significant to replace Pt.

In this context, the ultrahigh transmittance in the entire broad solar spectrum range, remarkable surface area ($2630 \text{ m}^2/\text{g}$), large electrical conductance and mobility, high thermal conductivity and appreciable mechanical properties of graphene made it a best alternative to Pt counter electrodes. This facilitates efficient exciton generation [56,91,229,230]. Hasin et al. first reported the capability of graphene to be used as counter electrodes in DSSCs [231]. The rigorous research on such graphene-based DSSCs has improved their efficiency to about 7–9.5% [2]. Considering the remarkable properties of graphene, the efficiency of graphene-based DSSCs can be predicted to increase much higher in the upcoming years.

Application of Graphene as Sensitizing Material in DSSCs

The tunable band gap of graphene by quantum confinement effect makes it ready to serve DSSCs as sensitizing material. Yan et al. first demonstrated this application of graphene in 2010 by synthesizing graphene quantum dots for sensitization of TiO_2 in DSSC [232]. As graphene quantum dots alone provided less efficiency, using them as co-sensitizer significantly raised the performance of common dyes. The high efficiency values of such DSSCs were found to be up to 7.95% [233,234].

Application of Graphene as Photoanode Additive in DSSCs

Since low-cost mass production of graphene sheets is quite challenging, researchers have found a way to utilize the limited amount of fabricated graphene by treating them as additives for photoanode materials. It was observed that this improved the electron transfer process and increased current in DSSCs [235]. Compared to carbon nanotubes (CNTs), graphene provides a much larger surface area leading to the efficient transfer of photogenerated electrons. This increased efficiency from 0.58 to 6.97% by adding graphene additive to the TiO_2 DSSC photoanode [218]. The same strategy yielded Madhavan et al. a DSSC with an efficiency of 7.6% using the graphene additive. This efficiency value was larger as compared to the efficiency of 6.3% without additives [236]. Guo et al. have provided the efficiencies of numerous graphene-based DSSCs in their in-depth analysis [235].

3.3.5. Application of Graphene in Quantum Dot SCs: Graphene-Based QD SC

To exploit the fascinating properties of quantum dots, quantum dot SCs (QD SCs) have attracted much attention from researchers. The facility of tuning band gap and optical absorption profiles of quantum dots by variation in their size made them suitable for the entire range of solar light harvesters [237–239]. Its unique electronic band structure can even help QD SCs to cross the Shockley–Queisser limit due to efficient hot electrons harvesting and multiple exciton generation [240,241].

Although QD SCs reached an efficiency of 44% theoretically, it is practically challenged by a higher recombination rate at TiO_2/QD junction and hole trapping between QDs. As a solution, many approaches like shell layers [242], doping anodes [243,244], hierarchical photoanodes [245], QD passivation [246], panchromatic sensitizers [247], Pt-free counter electrodes [248], etc., were employed. However, graphene attracted most of the interest as photoelectrode since it offered the best photocurrent and SC efficiency [249]. This was due to graphene's optimizable work function resulting in an excellent conductive network, large electron transfer rates, extended electron mean free path and charge escaping recombination [250]. Diao et al. developed graphene-based QD SC having configuration HNO_3 -doped graphene/GQDs/Si which resulted in optimum efficiency of 12.35% [94,251]. Moreover, their proposed SC showed excellent chemical and physical stability. This shows the capability of graphene to accelerate the development of QD SCs [2]. Nowadays, research is expanded to explore 3D graphene sheets for further improvement in QD SC efficiency [2,252].

3.3.6. Application of Graphene in Graphene/Semiconductor Van der Waals Heterostructure SCs

In principle, depositing graphene on any semiconductor naturally creates a Van der Waals Schottky diode [161,253–255]. Here, the graphene/semiconductor Schottky diode's barrier height can be easily tuned by shifting the Fermi level of the semiconductor and graphene. It is further benefited by the nature of the Van der Waals contact, small graphene screening length and low density of energy state near Dirac point [62,256]. This graphene/semiconductor Van der Waals heterostructure is constructively used to create high-efficiency SCs [5,204,257–259]. Technically, the gating effect is implemented to control the Fermi level tuning in such heterostructures. The graphene/InP heterostructure was recently been fabricated and its optimization was performed by shifting the Fermi level using the same gating effect. Its efficiency was 5.6% [260].

The state-of-the-art maximum efficiency of the graphene/semiconductor Schottky diode is 15.6% and is obtained for the graphene/Si system [261]. Li et al. fabricated graphene/GaAs heterostructure SC and optimized graphene's properties by doping to achieve appreciable efficiency of 15.5% [262]. By designing graphene–dielectric–graphene heterostructure and treating the top graphene layer as a gating electrode, they further enhanced the efficiency of their SC to 18.5%. The reason behind the high efficiency of this structure is the combined advantage of the antireflection property of the dielectric layer and the high transparency and the Fermi level tunability of graphene. They even demonstrated that their experimental results were in good agreement with the simulation output from the drift-diffusion simulation model that predicted efficiency above 23.8%. These studies indicate that high-efficiency SCs can be obtained using graphene/semiconductor Van der Waals heterostructures.

3.3.7. Application of Graphene in Tandem SCs: Graphene-Based Tandem SC

The tandem SCs or the multi-junction SCs are SC devices made by stacking two or more sub-cells together and varying their configuration between parallel and series connections in order to optimize their efficiency. These SCs are attracting much attention nowadays [263]. Mathematical models predict the theoretical efficiency of tandem SCs to reach up to 86% [93]. Hence, this concept is being applied to all types of SCs. Research efforts of various scientists have been summarized by Singh et al. in their work [93]. In recent research, graphene has also been incorporated to fabricate tandem SCs. However, graphene-based tandem SCs are still a relatively new area of research.

The V_{oc} of graphene-based tandem SCs is appreciably high (1.23 V to 1.69 V), but the efficiency reaches a maximum of up to 3.91% for ITO/PEDOT:PSS (40 nm)/PCDTBT:PCBM (1:4, 80 nm)/GO-Cs (2 nm)/Al (1 nm)/GO (2 nm)/MoO₃ (20 nm)/PCDTBT:PCBM (1:4, 80 nm)/Ca (30 nm)/Al (100 nm) SC structure of Chen et al. [264]. Here, the resistance of interconnecting layer between GO sheets was quite high. However, being the function of layer thickness, the interconnecting layer resistance value can be reduced. A point to be noted is that the resulting graphene-based tandem SCs exhibited efficiency higher as compared to SCs with the same sub-cells but lacking graphene as connecting layers [265]. Hence, the presence of graphene is shown to evidently increase overall SC efficiency. Owing to the attractive properties of both graphene and tandem SCs, their synergy is predicted to have great potential for future high-efficiency SCs.

3.3.8. Application of Graphene in Perovskite SCs: Graphene-Based PSC

The SCs that underwent the most rapid development after their discovery are the third-generation perovskite SCs (PSCs). From the time of their discovery by Kojima et al. in 2009, its efficiency rose from 3.9% to ~32% in just a few years. This owes to its most interesting properties such as large diffusion length of charge carriers, appreciable charge carrier mobility, direct band gap (1.5–2.3 eV) [266], small exciton binding energy, high absorption coefficient (10^4 cm^{-1}) [267], low manufacturing cost and eco-friendliness as compared to toxic lead-based perovskites [114,268–273]. These properties can even be

tuned, making it suitable for various applications. The summary of their development is demonstrated by Singh et al. [93].

In this context, the graphene-based PSCs are also performing well [85,274–283]. From the comparison table presented by Singh et al., one can conclude that the presence of graphene in PSCs often rises its efficiency [93]. Speaking quantitatively, Kuang et al. enhanced the performance of their SC from 14.8% to 28.7% just by inclusion of graphene layer into their SC [275]. Yeo et al. even demonstrated that the presence of reduced GO offered resistance against moisture and oxygen and increased the stability in PSCs [279]. Many studies have shown that graphene offers long-term stability to PSCs [284–293]. Li et al. found an increment in interface wettability due to the amphiphilic property of GO, reducing the contact angle to 0° and thereby, rising efficiency by 45.5% [93,280]. This can again be attributed to the combined effect of remarkable properties of both the graphene and PSCs. Hence, graphene-based PSCs are a very interesting future research area [294]. The various roles that graphene can play to contribute to higher PSC efficiency are discussed briefly below.

Application of Graphene as Charge Transport Layer in PSCs

Being ambipolar in nature, graphene and its derivatives can be used as both the ETL and HTL in PSCs depending on the type of graphene doping. Organic HTL was the most commonly used HTL but possessed few limitations. Hence, it was important to find an alternative to organic HTL PEDOT:PSS. With proper work function tuning, graphene easily outperformed organic PEDOT:PSS HTL and raised the PSC efficiency from 9.3% to 12.4% [295]. It can maintain a balance of work function and conductivity to act as an efficient HTL. Such SCs offered performance efficiency of 16.5% [276] and that too at low cost and improved PSC stability [296,297].

Like HTL, graphene has also proved to be an efficient ETL by lifting PSC efficiency from 13.5% to 14.5% [9]. Graphene offers fast electron extraction compared to other ETLs [9]. Along with an efficient transport layer, functionalized GO can also passivate traps present at perovskite layer grain boundaries. Thus, the defects and interfacial recombination centers are efficiently removed, thereby enhancing PSC efficiency up to as high as 18.75% [298]. Moreover, dispersing graphene flakes in mesoscopic TiO_2 helped scientists achieve a larger area of PSCs up to 50.6 cm^2 [9]. Hence, graphene-based PSCs are promising candidates for future high-efficiency stable SCs.

Application of Graphene as Electrodes in PSCs

Graphene has also been successfully applied as electrodes in PSCs. In order to make graphene an efficient electrode, it is appropriately doped to reduce sheet resistance as well as increase mobility and conductivity [299]. It was the bi-layer graphene that facilitated PSC efficiency of 12.02% and 11.65% when illuminated from the glass and graphene electrode sides, respectively [299]. To optimize the performance of graphene-based PSCs, multi-layer graphene films were tested. Finally, it was observed that it is the bi-layer graphene that offered balanced performance in terms of transmittance (90%) and sheet resistance ($140 \Omega/\text{sq}$) [299].

Sung et al. obtained the best efficiency of 17.1% for their graphene electrode-based PSC by tuning graphene's hydrophobic nature, sheet resistance and work function via doping [94,300]. Graphene electrodes also made PSCs more flexible [9]. PSCs can easily be thinned without considerable loss in photovoltaic power density and extinction coefficient [134,301]. This followed from the experimental observation that graphene remained intact and showed no cracks after repeated 1000 bending cycles, unlike other ITO-based SCs. It initially possessed 16.8% efficiency. After 1000 and 5000 bending cycles, the SC maintained efficiency > 90% and 85%, respectively, due to the presence of a graphene electrode [302]. Here, the ITO-based SCs reduced PSC efficiency by 50% after the same number of bending cycles [134]. Hence, graphene is seen to provide a due advantage to PSCs for achieving high efficiency, stability and mechanical strength.

Application of Graphene as Stabilizing Material in PSCs

To achieve its longer service lifetime, the durability and stability of graphene-based SCs need to be experimentally established under various environmental conditions. The biggest challenge that obstructs the commercialization of PSCs is their efficiency instability/degradation under a humid air environment. Being hydrophobic in nature, graphene can act as a barrier to the absorption of moisture. Hence, graphene was tested by growing it on the surface of PSCs. Results reveal that the PSCs retained 94% efficiency at 45% humidity even after 96 h of continuous illumination [114,303]. Impressively, PSCs with graphene as stabilizing material showed only 15% efficiency degradation after 500 h without encapsulation [304]. Furthermore, a PSC efficiency of 15% remained stable after a thermal aging test for 500 h at 85 °C as well as after light soaking under AM1.5 for 1000 h of continuous illumination [305]. In principle, due to the chemical inertness and super-hydrophobicity of graphene, PSCs gained strength and protection against chemical degradation and their performance is improved [306]. The durability and stability challenges of PSCs in real working conditions were also demonstrated to be resolved by defect, interfacial and compositional engineering of graphene [307]. The researchers Niazi et al. provide many more potential strategies to resolve challenges in graphene-based PSCs in their analysis [307].

3.3.9. Application of Graphene in Organic SCs: Graphene-Based OSC

Organic substances can be used to fabricate promising photovoltaic SCs since they can provide several advantages such as tunable physical properties, solution-processability, large surface area production, cost-effective synthesis and lightweight [308,309]. Moreover, being organic, they have the ability to prevent SC from degradation and provide stability against moisture, temperature and heat. Their large surface area production facilitates the synthesis of bulk heterojunction SCs [93].

Graphene's remarkable properties can be combined with that of organic SCs (OSCs) to form graphene-based OSCs [310]. Experimentalists observed reduced exciton recombination and enhanced charge transport leading to rise in graphene-based OSC efficiency [9]. Owing to its properties, graphene can be treated as an efficient electrode, charge transport layer and ternary material to contribute to high efficiencies of OSCs. These roles of graphene are briefly discussed below.

Application of Graphene as Electrodes in Graphene-Based OSCs

The potential of graphene to replace ITO as TCE is already mentioned above in detail. Graphene can replace ITO and provide better transparency, flexibility, desired work function, conductivity, higher material abundance, optimum surface morphology and low-cost processing [150,311]. Doping graphene can even enhance its conductivity, reduce sheet resistance and match its work function with adjacent layers. Its ambipolar nature widens its applications to an anode as well as a cathode [312] in OSCs depending on its doping profile.

If graphene's work function is greater than the HOMO of organic donor materials, Schottky contact is formed at the graphene/semiconductor junction and graphene behaves as an efficient anode. On the other hand, when its work function is less than the LUMO of organic acceptors, the ohmic contact necessary for electron collection is formed and it behaves as an efficient cathode. This mechanism is explored in detail in Section 3.1.2. Moreover, since TCEs are the uppermost SC layer, depositing TCE by radio-frequency plasma sputtering via ion bombardment, followed by post-deposition annealing, damages underlying organic layers [313–315]. Using graphene as an underlying layer prevents this SC damage against micro-cracks or fissures due to its mechanical strength properties. As graphene imparts flexibility to OSCs, the OSC device performance remained the same even after 100 bending cycles [316]. A good bending stability resulted in OSC efficiency reduction by just 8% after 1000 bending cycles [317].

Scientists tried to optimize OSCs by testing their performance with multi-layer graphene. They observed a decrease in the long-term stability of OSCs against oxygen and moisture for multi-layer graphene. Hence, the number of graphene layers was reduced to bi-layer or

tri-layer graphene [9,86]. The use of graphene as an anode improved OSC performance by 55% [318]. Doping even made graphene capable of OSC surface passivation by increasing wettability and hydrophilicity [89,319]. Research has improved graphene-based OSC efficiency by up to 3% [320]. However, consistent research endeavors can make graphene-based OSCs a promising photovoltaic technology.

Application of Graphene as Charge Transport Layer in Graphene-Based OSCs

The commonly used PEDOT:PSS organic HTL needed replacement owing to its high acidity (pH~1) and hygroscopic properties [321,322]. Inorganic materials can be the solution, but they are expensive in production. Hence, the most viable solution is graphene. It can be deposited through a cost-effective roll-to-roll process [323–327]. HTL requires a high work function to create a built-in electric field for efficient hole collection at the anode, whereas, ETL requires a low work function for efficient electron collection at the cathode. As the graphene is ambipolar and has tunable doping-dependent and thickness-dependent work function, sheet resistance and hydrophilicity, graphene and its derivatives are best suitable for ETL/HTL in OSCs [9,150]. Reduced GO has recently been applied as ETL in OSCs to improve its efficiency to 8.21% [328]. As HTL, fluorine-functionalized reduced GO yielded enhanced OSC performance of 8.6% [329]. Many studies reflect the potential of graphene as an efficient ETL/HTL [9].

Application of Graphene as Ternary Material in Graphene-Based OSCs

Ternary OSCs are OSCs with modified configurations depending on the ternary component: one donor/two acceptors, two donors/one acceptor and donor/non-volatile additive/acceptor type. Graphene and its derivatives can also be used as ternary compounds within the photoactive layer of ternary OSCs. The purpose of adding a third element in OSCs is to increase the charge transport and collection at the electrodes. This acts as a solution to inadequate charge transport issues in P3HT:PCBM OSCs. Due to the high electrical conductivity property, graphene fixes the imbalance of electron and hole mobility in OSCs to avoid charge trapping and efficient charge collection is made possible [9].

Graphene also enhances OSC efficiency. The physics behind it is that graphene expands the exciton dissociation area and increases the rapidity of electron transfer through it [330]. The effect of a small amount of graphene flakes treated as additives in OSCs is also studied. It was found to increase hole mobility and balance electron and hole mobilities to reduce charge trapping in graphene-based OSCs [331]. Graphene doping further led to betterment in charge transfer due to energy-level matching and reduction in recombination. This ultimately increased J_{sc} and OSC performance [332]. The efficiency of various OSCs underwent enhancement of ~18% and ~23% due to the presence of graphene [333,334]. Hence, graphene is termed as a potential candidate for high-efficiency OSCs.

3.3.10. Application of Graphene in Solid-State SCs: Graphene-Based Solid-State SC

A few researchers have even dedicated their studies to checking graphene as a junction material in solid-state SCs. As discussed earlier, graphene forms a Schottky junction at the graphene/semiconductor heterojunction. The sufficient difference in work function between graphene and n-type doped semiconductor creates substantial built-in potential [2]. Some graphene-based solid-state SCs are graphene-Si [159] and graphene-single CdS NW [204] solid-state SCs. Among many studies, graphene-based solid-state SC fabricated by Miao et al. showed commendable efficiency of 8.6% for graphene/Si solid-state SC [207]. They increased the efficiency of their proposed SC through graphene doping. This caused a shift in graphene's chemical potential which increased charge density and built-in potential in the device. It is regarded as one of the highest reported graphene-based solid-state SC efficiencies. This result indicates that further exploration of graphene's advantageous utilization in solid-state SCs can lead to highly efficient solid-state SCs [2].

Furthermore, to fully utilize the potential of graphene for enhancing SC efficiency, the role of graphene in various SC types needs to be explored further. It may be possible

by simulating graphene-based SCs for in-depth experimentally-inaccessible analysis and understanding of the exact working mechanism as performed by Dadashbeik et al. [335] and Arefinia et al. [336].

4. Conclusions and Perspective

Owing to the excellent attractive electrical, optical, chemical, thermal and mechanical properties of graphene, its scope of application has reached up to the photovoltaic technology sector. It has been found to be a reliable solution for many critical issues concerning non-graphene-based SCs as discussed in this paper. Intensive research on the application of graphene began from the time when two scientists Andre Geim and Konstantin Novoselov received the Nobel Prize award in Physics in 2010 for their ground-breaking experiment leading to the discovery of 2D graphene. Since then, graphene and its derivatives began to be applied in various SCs. A total of 10 different types of graphene-based SCs have been realized to date. In each type of SC, the graphene is observed to be capable of playing multiple roles such as an efficient anode, cathode, TCE, photoactive layer, buffer layer, acceptor layer, donor layer, ETL, HTL, electron/hole charge blocking layer, ternary material, SC stabilizing material, Schottky junction formation material, surface antireflective coating, passivating layer and recombination suppressant layer offering rapid charge transfer. Moreover, graphene is abundantly available, lightweight, flexible, eco-friendly and possesses minimal fabrication costs. Moreover, the bi-layer and tri-layer graphene have the potential to fairly uplift the SC performance appreciably as well as impart maximum stability to SC as compared to multi-layer graphene. Hence, the application of graphene in photovoltaic technology has a vast potential to revolutionize the industry.

As a future research direction, new techniques for controlled synthesis of high-quality graphene on a large scale and at low cost needs to be investigated. The effect of doping and the number of graphene layers on the stability and durability of graphene-based SCs under various environmental conditions can be queried. Moreover, the development of further understanding regarding chemical and physical interactions between graphene and different dopants is very essential. Also, new scientific ways to properly optimize graphene in labs with minimal damage need to be invented. Achieving a high doping concentration in graphene while maintaining its structural integrity is also a challenge. Additionally, the graphene/semiconductor interfacial engineering can potentially upgrade the power conversion efficiency of graphene-based SCs due to increment in its V_{oc} , J_{sc} and fill factor. Furthermore, the role of graphene in various SC technologies needs to be explored in greater detail to completely utilize graphene's potential for enhancing SC device efficiency. This can be performed by simulating graphene-based SCs for in-depth analysis of experimentally-inaccessible information and understanding its exact working mechanism on the nanoscale. Each fine research on graphene-based SC can be aimed to resolve various issues and advance our perception of graphene's impact on diverse SCs. Hence, the commercial application of graphene-based SCs can soon be realized in the near future. Thus, considering the evidence of the success of its application in graphene-based SCs, this review proposes enhanced focused research to discover/invent further hidden unexplored applications of this excellent material, graphene, for achieving next-level SCs.

Author Contributions: Conceptualization, S.S.B.; methodology, S.S.B.; validation, S.S.B., S.P., M.M.M. and P.K.P.; formal analysis, S.S.B., S.P., M.M.M. and P.K.P.; investigation, S.S.B.; resources, P.K.P. and S.S.B.; data curation, S.S.B.; writing—original draft preparation, S.S.B.; writing—review and editing, S.S.B.; visualization, S.S.B.; supervision, P.K.P.; project administration, P.K.P. All authors have read and agreed to the published version of the manuscript.

Funding: This research received no funding.

Data Availability Statement: Data that support the findings of this study is contained within the article.

Conflicts of Interest: The authors declare no competing interests.

References

1. Nadarajah, K.; Vakeesan, D. Solar energy for future world: A review. *Renew. Sustain. Energy Rev.* **2016**, *62*, 1092–1105.
2. Das, S.; Sudhagar, P.; Kang, Y.S.; Choi, W. Graphene synthesis and application for solar cells. *J. Mater. Res.* **2014**, *29*, 299–319. [[CrossRef](#)]
3. Novoselov, K.S.; Geim, A.K.; Morozov, S.V.; Jiang, D.E.; Zhang, Y.; Dubonos, S.V.; Grigorieva, I.V.; Firsov, A.A. Electric field effect in atomically thin carbon films. *Science* **2004**, *306*, 666–669. [[CrossRef](#)] [[PubMed](#)]
4. Burghard, M.; Hagen, K.; Klaus, K. Carbon-based field-effect transistors for nanoelectronics. *Adv. Mater.* **2009**, *21*, 2586–2600. [[CrossRef](#)]
5. Behura, S.K.; Mahala, P.; Nayak, S.; Yang, Q.; Mukhopadhyay, I.; Jani, O. Fabrication of bi-layer graphene and theoretical simulation for its possible application in thin film solar cell. *J. Nanosci. Nanotechnol.* **2014**, *14*, 3022–3027. [[CrossRef](#)] [[PubMed](#)]
6. Tamandani, S.; Darvish, G.; Faez, R. Analytical calculation of energy levels of mono-and bilayer graphene quantum dots used as light absorber in solar cells. *Appl. Phys. A* **2016**, *122*, 37. [[CrossRef](#)]
7. Radamson, H.H. Graphene. In *Springer Handbook of Electronic and Photonic Materials*; Springer: Berlin/Heidelberg, Germany, 2017; p. 1.
8. Bahri, M.; Gebre, S.H.; Elaguech, M.A.; Dajan, F.T.; Sendeku, M.G.; Tlili, C.; Wang, D. Recent advances in chemical vapour deposition techniques for graphene-based nanoarchitectures: From synthesis to contemporary applications. *Coord. Chem. Rev.* **2023**, *475*, 214910. [[CrossRef](#)]
9. Das, S.; Pandey, D.; Thomas, J.; Roy, T. The role of graphene and other 2D materials in solar photovoltaics. *Adv. Mater.* **2019**, *31*, 1802722. [[CrossRef](#)]
10. Nandi, A.; Majumdar, S.; Datta, S.K.; Saha, H.; Hossain, S.M. Optical and electrical effects of thin reduced graphene oxide layers on textured wafer-based c-Si solar cells for enhanced performance. *J. Mater. Chem. C* **2017**, *5*, 1920–1934. [[CrossRef](#)]
11. Wendler, F.; Knorr, A.; Malic, E. Carrier multiplication in graphene under Landau quantization. *Nat. Commun.* **2014**, *5*, 3703. [[CrossRef](#)]
12. Balandin, A.A. Thermal properties of graphene and nanostructured carbon materials. *Nat. Mater.* **2011**, *10*, 569–581. [[CrossRef](#)] [[PubMed](#)]
13. Akinwande, D.; Brennan, C.J.; Bunch, J.S.; Egberts, P.; Felts, J.R.; Gao, H.; Huang, R.; Kim, J.S.; Li, T.; Li, Y.; et al. A review on mechanics and mechanical properties of 2D materials—Graphene and beyond. *Extrem. Mech. Lett.* **2017**, *13*, 42–77. [[CrossRef](#)]
14. Papageorgiou, D.G.; Ian, A.K.; Robert, J.Y. Mechanical properties of graphene and graphene-based nanocomposites. *Prog. Mater. Sci.* **2017**, *90*, 75–127. [[CrossRef](#)]
15. Behura, S.K.; Mahala, P.; Ray, A.; Mukhopadhyay, I.; Jani, O. Theoretical simulation of photovoltaic response of graphene-on-semiconductors. *Appl. Phys. A* **2013**, *111*, 1159–1163. [[CrossRef](#)]
16. Craighead, H.G.; Julian, C.; Hackwood, S. New display based on electrically induced index-matching in an inhomogeneous medium. *Appl. Phys. Lett.* **1982**, *40*, 22–24. [[CrossRef](#)]
17. Xia, S.; Huang, W.; Yan, W.; Yuan, X.; Chen, X.; Liu, L.; Fu, L.; Zhu, Y.; Huang, Q.; Wu, Y.; et al. A Separator Modified with Rutile Titania and Three-Dimensional Interconnected Graphene-Like Carbon for Advanced Li–S Batteries. *ChemElectroChem* **2022**, *9*, e202200301. [[CrossRef](#)]
18. Wang, G.; Shen, X.; Yao, J.; Park, J. Graphene nanosheets for enhanced lithium storage in lithium ion batteries. *Carbon* **2009**, *47*, 2049–2053. [[CrossRef](#)]
19. Cai, X.; Lai, L.; Shen, Z.; Lin, J. Graphene and graphene-based composites as Li-ion battery electrode materials and their application in full cells. *J. Mater. Chem. A* **2017**, *5*, 15423–15446. [[CrossRef](#)]
20. Cheng, Q.; Okamoto, Y.; Tamura, N.; Tsuji, M.; Maruyama, S.; Matsuo, Y. Graphene-like-graphite as fast-chargeable and high-capacity anode materials for lithium ion batteries. *Sci. Rep.* **2017**, *7*, 14782. [[CrossRef](#)]
21. Wang, F.; Wang, C.; Zhao, Y.; Liu, Z.; Chang, Z.; Fu, L.; Zhu, Y.; Wu, Y.; Zhao, D. A quasi-solid-state Li-ion capacitor based on porous TiO₂ hollow microspheres wrapped with graphene nanosheets. *Small* **2016**, *12*, 6207–6213. [[CrossRef](#)]
22. Wang, F.; Liu, Z.; Yuan, X.; Mo, J.; Li, C.; Fu, L.; Zhu, Y.; Wu, X.; Wu, Y. A quasi-solid-state Li-ion capacitor with high energy density based on Li₃VO₄/carbon nanofibers and electrochemically-exfoliated graphene sheets. *J. Mater. Chem. A* **2017**, *5*, 14922–14929. [[CrossRef](#)]
23. Ke, Q.; Wang, J. Graphene-based materials for supercapacitor electrodes—A review. *J. Mater.* **2016**, *2*, 37–54. [[CrossRef](#)]
24. Tan, Y.B.; Jong-Min, L. Graphene for supercapacitor applications. *J. Mater. Chem. A* **2013**, *1*, 14814–14843. [[CrossRef](#)]

25. Yang, W.; Ni, M.; Ren, X.; Tian, Y.; Li, N.; Su, Y.; Zhang, X. Graphene in supercapacitor applications. *Curr. Opin. Colloid Interface Sci.* **2015**, *20*, 416–428. [[CrossRef](#)]
26. Yang, H.; Kannappan, S.; Pandian, A.S.; Jang, J.H.; Lee, Y.S.; Lu, W. Graphene supercapacitor with both high power and energy density. *Nanotechnology* **2017**, *28*, 445401. [[CrossRef](#)]
27. Vivekchand, S.R.C.; Rout, C.S.; Subrahmanyam, K.S.; Govindaraj, A.; Rao, C.N.R. Graphene-based electrochemical supercapacitors. *J. Chem. Sci.* **2008**, *120*, 9–13. [[CrossRef](#)]
28. Ou, Z.; An, Z.; Ma, Z.; Li, N.; Han, Y.; Yang, G.; Jiang, Q.; Chen, Q.; Chu, W.; Wang, S.; et al. 3D Porous Graphene-like Carbons Encaged Single-Atom-Based Pt for Ultralow Loading and High-Performance Fuel Cells. *ACS Catal.* **2023**, *13*, 1856–1862. [[CrossRef](#)]
29. Choi, H.J.; Jung, S.M.; Seo, J.M.; Chang, D.W.; Dai, L.; Baek, J.B. Graphene for energy conversion and storage in fuel cells and supercapacitors. *Nano Energy* **2012**, *1*, 534–551. [[CrossRef](#)]
30. Shaari, N.; Kamarudin, S.K. Graphene in electrocatalyst and proton conduction membrane in fuel cell applications: An overview. *Renew. Sustain. Energy Rev.* **2017**, *69*, 862–870. [[CrossRef](#)]
31. Farooqui, U.R.; Abdul, L.A.; Hamid, N.A. Graphene oxide: A promising membrane material for fuel cells. *Renew. Sustain. Energy Rev.* **2018**, *82*, 714–733. [[CrossRef](#)]
32. Li, J.; Chen, J.; Shen, B.; Yan, X.; Xue, Q. Temperature dependence of the field emission from the few-layer graphene film. *Appl. Phys. Lett.* **2011**, *99*, 163103. [[CrossRef](#)]
33. Ye, D.; Moussa, S.; Ferguson, J.D.; Baski, A.A.; El-Shall, M.S. Highly efficient electron field emission from graphene oxide sheets supported by nickel nanotip arrays. *Nano Lett.* **2012**, *12*, 1265–1268. [[CrossRef](#)] [[PubMed](#)]
34. Dikin, D.A.; Stankovich, S.; Zimney, E.J.; Piner, R.D.; Dommett, G.H.; Evmenenko, G.; Nguyen, S.T.; Ruoff, R.S. Preparation and characterization of graphene oxide paper. *Nature* **2007**, *448*, 457–460. [[CrossRef](#)] [[PubMed](#)]
35. Li, G.L.; Liu, G.; Li, M.; Wan, D.; Neoh, K.G.; Kang, E.T. Organo- and water-dispersible graphene oxide–polymer nanosheets for organic electronic memory and gold nanocomposites. *J. Phys. Chem. C* **2010**, *114*, 12742–12748. [[CrossRef](#)]
36. Zande, A.M.V.D.; Barton, R.A.; Alden, J.S.; Ruiz-Vargas, C.S.; Whitney, W.S.; Pham, P.H.; Park, J.; Parpia, J.M.; Craighead, H.G.; McEuen, P.L. Large-scale arrays of single-layer graphene resonators. *Nano Lett.* **2010**, *10*, 4869–4873. [[CrossRef](#)]
37. Schedin, F.; Geim, A.K.; Morozov, S.V.; Hill, E.W.; Blake, P.; Katsnelson, M.I.; Novoselov, K.S. Detection of individual gas molecules adsorbed on graphene. *Nat. Mater.* **2007**, *6*, 652–655. [[CrossRef](#)] [[PubMed](#)]
38. Xia, F.; Mueller, T.; Lin, Y.M.; Valdes-Garcia, A.; Avouris, P. Ultrafast graphene photodetector. *Nat. Nanotechnol.* **2009**, *4*, 839–843. [[CrossRef](#)]
39. Wang, J.X.; Lai, H.; Zhong, M.; Liu, X.; Chen, Y.; Yao, S. Design and Scalable Fabrication of Liquid Metal and Nano-Sheet Graphene Hybrid Phase Change Materials for Thermal Management. *Small Methods* **2023**, 2300139. [[CrossRef](#)]
40. Palacios, T. Thinking outside the silicon box. *Nat. Nanotechnol.* **2011**, *6*, 464–465. [[CrossRef](#)]
41. Han, W.; Kawakami, R.K.; Gmitra, M.; Fabian, J. Graphene spintronics. *Nat. Nanotechnol.* **2014**, *9*, 794–807. [[CrossRef](#)]
42. Yu, X.; Cheng, H.; Zhang, M.; Zhao, Y.; Qu, L.; Shi, G. Graphene-based smart materials. *Nat. Rev. Mater.* **2017**, *2*, 17046. [[CrossRef](#)]
43. Song, Y.; Luo, Y.; Zhu, C.; Li, H.; Du, D.; Lin, Y. Recent advances in electrochemical biosensors based on graphene two-dimensional nanomaterials. *Biosens. Bioelectron.* **2016**, *76*, 195–212. [[CrossRef](#)] [[PubMed](#)]
44. Kumar, S.; Duesberg, G.S.; Pratap, R.; Raghavan, S. Graphene field emission devices. *Appl. Phys. Lett.* **2014**, *105*, 103107. [[CrossRef](#)]
45. Ahn, J.-H.; Byung, H.H. Graphene for displays that bend. *Nat. Nanotechnol.* **2014**, *9*, 737–738. [[CrossRef](#)] [[PubMed](#)]
46. Polat, E.O.; Balci, O.; Kakenov, N.; Uzlu, H.B.; Kocabas, C.; Dahiya, R. Synthesis of large area graphene for high performance in flexible optoelectronic devices. *Sci. Rep.* **2015**, *5*, 16744. [[CrossRef](#)] [[PubMed](#)]
47. Kostarelos, K.; Vincent, M.; Hebert, C.; Garrido, J.A. Graphene in the design and engineering of next-generation neural interfaces. *Adv. Mater.* **2017**, *29*, 1700909. [[CrossRef](#)]
48. Nguyen, B.H.; Nguyen, V.H. Promising applications of graphene and graphene-based nanostructures. *Adv. Nat. Sci. Nanosci. Nanotechnol.* **2016**, *7*, 023002. [[CrossRef](#)]
49. Liao, L.; Xiangfeng, D. Graphene for radio frequency electronics. *Mater. Today* **2012**, *15*, 328–338. [[CrossRef](#)]
50. Zhu, W.; Perebeinos, V.; Freitag, M.; Avouris, P. Carrier scattering, mobilities, and electrostatic potential in monolayer, bilayer, and trilayer graphene. *Phys. Rev. B* **2009**, *80*, 235402. [[CrossRef](#)]
51. Nandi, A.; Dhar, S.; Majumdar, S.; Saha, H.; Hossain, S.M. Performance Enhancement of Solar Cell by Incorporating Bilayer RGO-ITO Smart Conducting Antireflection Coating. *Glob. Chall.* **2019**, *3*, 1800109. [[CrossRef](#)]
52. Becerril, H.A.; Mao, J.; Liu, Z.; Stoltenberg, R.M.; Bao, Z.; Chen, Y. Evaluation of solution-processed reduced graphene oxide films as transparent conductors. *ACS Nano* **2008**, *2*, 463–470. [[CrossRef](#)] [[PubMed](#)]
53. Kim, K.S.; Zhao, Y.; Jang, H.; Lee, S.Y.; Kim, J.M.; Kim, K.S.; Ahn, J.H.; Kim, P.; Choi, J.Y.; Hong, B.H. Large-scale pattern growth of graphene films for stretchable transparent electrodes. *Nature* **2009**, *457*, 706–710. [[CrossRef](#)]
54. Huang, H.; Chen, W.; Chen, S.; Wee, A.T.S. Bottom-up growth of epitaxial graphene on 6H-SiC (0001). *ACS Nano* **2008**, *2*, 2513–2518. [[CrossRef](#)] [[PubMed](#)]
55. Tung, V.C.; Allen, M.J.; Yang, Y.; Kaner, R.B. High-throughput solution processing of large-scale graphene. *Nat. Nanotechnol.* **2009**, *4*, 25–29. [[CrossRef](#)] [[PubMed](#)]

56. Reina, A.; Jia, X.; Ho, J.; Nezich, D.; Son, H.; Bulovic, V.; Dresselhaus, M.S.; Kong, J. Large area, few-layer graphene films on arbitrary substrates by chemical vapor deposition. *Nano Lett.* **2009**, *9*, 30–35. [[CrossRef](#)] [[PubMed](#)]
57. Shi, P.C.; Guo, J.P.; Liang, X.; Cheng, S.; Zheng, H.; Wang, Y.; Chen, C.H.; Xiang, H.F. Large-scale production of high-quality graphene sheets by a non-electrified electrochemical exfoliation method. *Carbon* **2018**, *126*, 507–513. [[CrossRef](#)]
58. Li, J.; Yan, H.; Dang, D.; Wei, W.; Meng, L. Salt and water co-assisted exfoliation of graphite in organic solvent for efficient and large scale production of high-quality graphene. *J. Colloid Interface Sci.* **2019**, *535*, 92–99. [[CrossRef](#)]
59. Islam, A.; Mukherjee, B.; Pandey, K.K.; Keshri, A.K. Ultra-fast, chemical-free, mass production of high quality exfoliated graphene. *ACS Nano* **2021**, *15*, 1775–1784. [[CrossRef](#)]
60. Shi, Z.; He, P.; Wang, N.; Liu, Y.; Chen, X.; Li, Y.; Ding, G.; Yu, Q.; Xie, X. Bubble-Mediated Mass Production of Graphene: A Review. *Adv. Funct. Mater.* **2022**, *32*, 2203124. [[CrossRef](#)]
61. Qiao, C.; Che, J.; Wang, J.; Wang, X.; Qiu, S.; Wu, W.; Chen, Y.; Zu, X.; Tang, Y. Cost effective production of high quality multilayer graphene in molten Sn bubble column by using CH₄ as carbon source. *J. Alloys Compd.* **2023**, *930*, 167495. [[CrossRef](#)]
62. Geim, A.K.; Novoselov, K.S. The rise of graphene. *Nat. Mater.* **2007**, *6*, 183–191. [[CrossRef](#)] [[PubMed](#)]
63. Viculis, L.M.; Mack, J.J.; Kaner, R.B. A Chemical Route to Carbon Nanoscrolls. *Science* **2003**, *299*, 1361. [[CrossRef](#)] [[PubMed](#)]
64. Hernandez, Y.; Nicolosi, V.; Lotya, M.; Blighe, F.M.; Sun, Z.; De, S.; McGovern, I.T.; Holland, B.; Byrne, M.; Gun'Ko, Y.K.; et al. High-yield production of graphene by liquid-phase exfoliation of graphite. *Nat. Nanotechnol.* **2008**, *3*, 563–568. [[CrossRef](#)]
65. Wintterlin, J.; Bocquet, M.-L. Graphene on metal surfaces. *Surf. Sci.* **2009**, *603*, 1841–1852. [[CrossRef](#)]
66. Berger, C.; Song, Z.; Li, T.; Li, X.; Ogbazghi, A.Y.; Feng, R.; Dai, Z.; Marchenkov, A.N.; Conrad, E.H.; First, P.N.; et al. Ultrathin epitaxial graphite: 2D electron gas properties and a route toward graphene-based nanoelectronics. *J. Phys. Chem. B* **2004**, *108*, 19912–19916. [[CrossRef](#)]
67. Hupalo, M.; Conrad, E.; Tringides, M.C. Growth mechanism for epitaxial graphene on vicinal 6H-SiC (0001) surfaces. *arXiv* **2008**, arXiv:0809.3619.
68. De Heer, W.A.; Berger, C.; Wu, X.; First, P.N.; Conrad, E.H.; Li, X.; Li, T.; Sprinkle, M.; Hass, J.; Sadowski, M.L.; et al. Epitaxial graphene. *Solid State Commun.* **2007**, *143*, 92–100. [[CrossRef](#)]
69. Kymakis, E.; Stratakis, E.; Stylianakis, M.M.; Koudoumas, E.; Fotakis, C. Spin coated graphene films as the transparent electrode in organic photovoltaic devices. *Thin Solid Film.* **2011**, *520*, 1238–1241. [[CrossRef](#)]
70. Wang, X.; Linjie, Z.; Klaus, M. Transparent, conductive graphene electrodes for dye-sensitized solar cells. *Nano Lett.* **2008**, *8*, 323–327. [[CrossRef](#)]
71. Lin, J.Y.; Chan, C.Y.; Chou, S.W. Electrophoretic deposition of transparent MoS₂-graphene nanosheet composite films as counter electrodes in dye-sensitized solar cells. *ChemComm* **2013**, *49*, 1440–1442.
72. Li, D.; Müller, M.B.; Gilje, S.; Kaner, R.B.; Wallace, G.G. Processable aqueous dispersions of graphene nanosheets. *Nat. Nanotechnol.* **2008**, *3*, 101–105. [[CrossRef](#)] [[PubMed](#)]
73. Eda, G.; Lin, Y.Y.; Miller, S.; Chen, C.W.; Su, W.F.; Chhowalla, M. Transparent and conducting electrodes for organic electronics from reduced graphene oxide. *Appl. Phys. Lett.* **2008**, *92*, 209. [[CrossRef](#)]
74. Ishikawa, R.; Bando, M.; Wada, H.; Kurokawa, Y.; Sandhu, A.; Konagai, M. Layer-by-layer assembled transparent conductive graphene films for silicon thin-film solar cells. *Jpn. J. Appl. Phys.* **2012**, *51*, 11PF01. [[CrossRef](#)]
75. Zhu, Y.; Cai, W.; Piner, R.D.; Velamakanni, A.; Ruoff, R.S. Transparent self-assembled films of reduced graphene oxide platelets. *Appl. Phys. Lett.* **2009**, *95*, 103104. [[CrossRef](#)]
76. Chen, C.; Yang, Q.H.; Yang, Y.; Lv, W.; Wen, Y.; Hou, P.X.; Wang, M.; Cheng, H.M. Self-assembled free-standing graphite oxide membrane. *Adv. Mater.* **2009**, *21*, 3007–3011. [[CrossRef](#)]
77. Kim, J.; Cote, L.J.; Kim, F.; Yuan, W.; Shull, K.R.; Huang, J. Graphene oxide sheets at interfaces. *J. Am. Chem. Soc.* **2010**, *132*, 8180–8186. [[CrossRef](#)]
78. Cote, L.J.; Franklin, K.; Jiaying, H. Langmuir–Blodgett assembly of graphite oxide single layers. *J. Am. Chem. Soc.* **2009**, *131*, 1043–1049. [[CrossRef](#)]
79. Li, X.; Zhang, R.; Yu, W.; Wang, K.; Wei, J.; Wu, D.; Cao, A.; Li, Z.; Cheng, Y.; Zheng, Q.; et al. Stretchable and highly sensitive graphene-on-polymer strain sensors. *Sci. Rep.* **2012**, *2*, 870. [[CrossRef](#)]
80. Li, X.; Cai, W.; An, J.; Kim, S.; Nah, J.; Yang, D.; Piner, R.; Velamakanni, A.; Jung, I.; Tutuc, E.; et al. Large-area synthesis of high-quality and uniform graphene films on copper foils. *Science* **2009**, *324*, 1312–1314. [[CrossRef](#)]
81. Das, S.; Sudhagar, P.; Verma, V.; Song, D.; Ito, E.; Lee, S.Y.; Kang, Y.S.; Choi, W. Amplifying charge-transfer characteristics of graphene for triiodide reduction in dye-sensitized solar cells. *Adv. Funct. Mater.* **2011**, *21*, 3729–3736. [[CrossRef](#)]
82. Chandrashekar, B.N.; Smitha, A.S.; Wu, Y.; Cai, N.; Li, Y.; Huang, Z.; Wang, W.; Shi, R.; Wang, J.; Liu, S.; et al. A universal stamping method of graphene transfer for conducting flexible and transparent polymers. *Sci. Rep.* **2019**, *9*, 3999. [[CrossRef](#)] [[PubMed](#)]
83. Verma, V.P.; Das, S.; Lahiri, I.; Choi, W. Large-area graphene on polymer film for flexible and transparent anode in field emission device. *Appl. Phys. Lett.* **2010**, *96*, 203108. [[CrossRef](#)]
84. Bae, S.; Kim, H.; Lee, Y.; Xu, X.; Park, J.S.; Zheng, Y.; Balakrishnan, J.; Lei, T.; Ri Kim, H.; Song, Y.I.; et al. Roll-to-roll production of 30-inch graphene films for transparent electrodes. *Nat. Nanotechnol.* **2010**, *5*, 574–578. [[CrossRef](#)]
85. Ahmed, D.S.; Mohammed, M.K.; Majeed, S.M. Green synthesis of eco-friendly graphene quantum dots for highly efficient perovskite solar cells. *ACS Appl. Energy Mater.* **2020**, *3*, 10863–10871. [[CrossRef](#)]

86. Koo, D.; Jung, S.; Seo, J.; Jeong, G.; Choi, Y.; Lee, J.; Lee, S.M.; Cho, Y.; Jeong, M.; Lee, J.; et al. Flexible organic solar cells over 15% efficiency with polyimide-integrated graphene electrodes. *Joule* **2020**, *4*, 1021–1034. [[CrossRef](#)]
87. Díez-Pascual, A.M.; Abbas, R. Graphene-based polymer composites for flexible electronic applications. *Micromachines* **2022**, *13*, 1123. [[CrossRef](#)] [[PubMed](#)]
88. Al Busaidi, H.; Suhail, A.; Jenkins, D.; Pan, G. Developed graphene/Si Schottky junction solar cells based on the top-window structure. *Carbon Trends* **2023**, *10*, 100247. [[CrossRef](#)]
89. Wang, Y.; Tong, S.W.; Xu, X.F.; Özyilmaz, B.; Loh, K.P. Interface engineering of layer-by-layer stacked graphene anodes for high-performance organic solar cells. *Adv. Mater.* **2011**, *23*, 1514–1518. [[CrossRef](#)]
90. Li, P.; Chen, C.; Zhang, J.; Li, S.; Sun, B.; Bao, Q. Graphene-based transparent electrodes for hybrid solar cells. *Front. Mater.* **2014**, *1*, 26. [[CrossRef](#)]
91. Li, X.; Zhu, Y.; Cai, W.; Borysiak, M.; Han, B.; Chen, D.; Piner, R.D.; Colombo, L.; Ruoff, R.S. Transfer of large-area graphene films for high-performance transparent conductive electrodes. *Nano Lett.* **2009**, *9*, 4359–4363. [[CrossRef](#)]
92. Zhu, Y.; Murali, S.; Cai, W.; Li, X.; Suk, J.W.; Potts, J.R.; Ruoff, R.S. Graphene and graphene oxide: Synthesis, properties, and applications. *Adv. Mater.* **2010**, *22*, 3906–3924. [[CrossRef](#)] [[PubMed](#)]
93. Singh, E.; Hari, S.N. Graphene-based bulk-heterojunction solar cells: A review. *J. Nanosci. Nanotechnol.* **2015**, *15*, 6237–6278. [[CrossRef](#)]
94. Shin, D.H.; Suk-Ho, C. Use of graphene for solar cells. *J. Korean Phys. Soc.* **2018**, *72*, 1442–1453. [[CrossRef](#)]
95. Parvez, K.; Rongjin, L.; Klaus, M. Graphene as transparent electrodes for solar cells. *Nanocarbons Adv. Energy Convers.* **2015**, 249–280.
96. Liu, Z.; Shu, P.L.; Feng, Y. Functionalized graphene and other two-dimensional materials for photovoltaic devices: Device design and processing. *Chem. Soc. Rev.* **2015**, *15*, 5638–5679. [[CrossRef](#)] [[PubMed](#)]
97. Wei, Y.; Zhang, Y.; Liu, Z.; Wang, Y.; Ke, F.; Meng, J.; Guo, Y.; Ma, P.; Feng, Q.; Gan, Z. High quality and large-scale manually operated monolayer graphene pasters. *Nanotechnology* **2014**, *25*, 275704. [[CrossRef](#)] [[PubMed](#)]
98. Ishikawa, R.; Yamazaki, S.; Watanabe, S.; Tsuboi, N. Layer dependency of graphene layers in perovskite/graphene solar cells. *Carbon* **2021**, *172*, 597–601. [[CrossRef](#)]
99. La Notte, L.; Villari, E.; Palma, A.L.; Sacchetti, A.; Giangregorio, M.M.; Bruno, G.; Di Carlo, A.; Bianco, G.V.; Reale, A. Laser-patterned functionalized CVD-graphene as highly transparent conductive electrodes for polymer solar cells. *Nanoscale* **2017**, *9*, 62–69. [[CrossRef](#)]
100. Arefinia, Z.; Asghar, A. A new modeling approach for graphene based silicon nanowire Schottky junction solar cells. *J. Renew. Sustain. Energy* **2014**, *6*, 043132. [[CrossRef](#)]
101. Cho, J.H.; Na, S.R.; Park, S.; Akinwande, D.; Liechti, K.M.; Cullinan, M.A. Controlling the number of layers in graphene using the growth pressure. *Nanotechnology* **2019**, *30*, 235602. [[CrossRef](#)]
102. Lin, Z.; Ye, X.; Han, J.; Chen, Q.; Fan, P.; Zhang, H.; Xie, D.; Zhu, H.; Zhong, M. Precise control of the number of layers of graphene by picosecond laser thinning. *Sci. Rep.* **2015**, *5*, 11662. [[CrossRef](#)]
103. Tu, Z.; Liu, Z.; Li, Y.; Yang, F.; Zhang, L.; Zhao, Z.; Xu, C.; Wu, S.; Liu, H.; Yang, H.; et al. Controllable growth of 1–7 layers of graphene by chemical vapour deposition. *Carbon* **2014**, *73*, 252–258. [[CrossRef](#)]
104. Negishi, R.; Hirano, H.; Ohno, Y.; Maehashi, K.; Matsumoto, K.; Kobayashi, Y. Layer-by-layer growth of graphene layers on graphene substrates by chemical vapor deposition. *Thin Solid Film.* **2011**, *519*, 6447–6452. [[CrossRef](#)]
105. Sun, J.; Liu, H.; Chen, X.; Evans, D.G.; Yang, W.; Duan, X. Synthesis of graphene nanosheets with good control over the number of layers within the two-dimensional galleries of layered double hydroxides. *Chem. Commun.* **2012**, *48*, 8126–8128. [[CrossRef](#)]
106. Wang, W.; Wang, Y.; Gao, Y.; Zhao, Y. Control of number of graphene layers using ultrasound in supercritical CO₂ and their application in lithium-ion batteries. *J. Supercrit. Fluids* **2014**, *85*, 95–101. [[CrossRef](#)]
107. Ihm, K.; Lim, J.T.; Lee, K.J.; Kwon, J.W.; Kang, T.H.; Chung, S.; Bae, S.; Kim, J.H.; Hong, B.H.; Yeom, G.Y. Number of graphene layers as a modulator of the open-circuit voltage of graphene-based solar cell. *Appl. Phys. Lett.* **2010**, *97*, 032113. [[CrossRef](#)]
108. Wang, H.; Thandavarayan, M.; Xin, W. Review on recent progress in nitrogen-doped graphene: Synthesis, characterization, and its potential applications. *ACS Catal.* **2012**, *2*, 781–794. [[CrossRef](#)]
109. Wang, X.; Sun, G.; Routh, P.; Kim, D.H.; Huang, W.; Chen, P. Heteroatom-doped graphene materials: Syntheses, properties and applications. *Chem. Soc. Rev.* **2014**, *43*, 7067–7098. [[CrossRef](#)]
110. Yang, N.; Yang, D.; Chen, L.; Liu, D.; Cai, M.; Fan, X. Design and adjustment of the graphene work function via size, modification, defects, and doping: A first-principle theory study. *Nanoscale Res. Lett.* **2017**, *12*, 642. [[CrossRef](#)]
111. Kwon, K.C.; Kyoung, S.C.; Soo, Y.K. Increased work function in few-layer graphene sheets via metal chloride doping. *Adv. Funct. Mater.* **2012**, *22*, 4724–4731. [[CrossRef](#)]
112. Shi, Y.; Kim, K.K.; Reina, A.; Hofmann, M.; Li, L.J.; Kong, J. Work function engineering of graphene electrode via chemical doping. *ACS Nano* **2010**, *4*, 2689–2694. [[CrossRef](#)] [[PubMed](#)]
113. Garg, R.; Dutta, N.K.; Roy Choudhury, N. Work function engineering of graphene. *Nanomaterials* **2014**, *4*, 267–300. [[CrossRef](#)] [[PubMed](#)]
114. Patel, P.K. Device simulation of highly efficient eco-friendly CH₃NH₃SnI₃ perovskite solar cell. *Sci. Rep.* **2021**, *11*, 3082. [[CrossRef](#)] [[PubMed](#)]

115. Hu, Z.; Zhao, Y.; Zou, W.; Lu, Q.; Liao, J.; Li, F.; Shang, M.; Lin, L.; Liu, Z. Doping of Graphene Films: Open the way to Applications in Electronics and Optoelectronics. *Adv. Funct. Mater.* **2022**, *32*, 2203179. [[CrossRef](#)]
116. Yu, X.; Yang, L.; Lv, Q.; Xu, M.; Chen, H.; Yang, D. The enhanced efficiency of graphene–silicon solar cells by electric field doping. *Nanoscale* **2015**, *7*, 7072–7077. [[CrossRef](#)] [[PubMed](#)]
117. Escoffier, W.; Poumirol, J.; Yang, R.; Goiran, M.; Raquet, B.; Broto, J. Electric field doping of few-layer graphene. *Phys. B Condens. Matter* **2010**, *405*, 1163–1167. [[CrossRef](#)]
118. Pinto, H.; Markevich, A. Electronic and electrochemical doping of graphene by surface absorbates. *Beilstein J. Nanotechnol.* **2014**, *5*, 1842–1848. [[CrossRef](#)] [[PubMed](#)]
119. Yu, Y.J.; Zhao, Y.; Ryu, S.; Brus, L.E.; Kim, K.S.; Kim, P. Tuning the graphene work function by electric field effect. *Nano Lett.* **2009**, *9*, 3430–3434. [[CrossRef](#)]
120. Liu, L.; Jia, L.; Huang, Y.; Zhang, Y.; Yu, W. High-performance vertical graphene nanowall/silicon Schottky junction solar cells with Nafion doping and plasma etching. *J. Alloys Compd.* **2023**, *939*, 168765. [[CrossRef](#)]
121. Shamim, S.U.D.; Piya, A.A.; Rahman, M.S.; Hasan, S.M.; Hossain, M.K.; Ahmed, F. Tuning the electrochemical behavior of graphene oxide and reduced graphene oxide via doping hexagonal BN for high capacity negative electrode for Li and Na ion batteries. *Phys. Chem. Chem. Phys.* **2023**, *25*, 4047–4061. [[CrossRef](#)]
122. Ubhi, M.K.; Kaur, M.; Grewal, J.K.; Sharma, V.K. Phosphorous-and boron-doped graphene-based nanomaterials for energy-related applications. *Materials* **2023**, *16*, 1155. [[CrossRef](#)] [[PubMed](#)]
123. Mollaamin, F.; Majid, M. Doping of Graphene Nanostructure with Iron, Nickel and Zinc as Selective Detector for the Toxic Gas Removal: A Density Functional Theory Study. *C* **2023**, *9*, 20. [[CrossRef](#)]
124. Kandula, S.; Youn, B.S.; Cho, J.; Lim, H.K.; Son, J.G. FeS₂@ NC nanorattles encapsulated in N/S dual-doped graphene/carbon nanotube network composites for high performance and high rate capability anodes of sodium-ion batteries. *Chem. Eng. J.* **2022**, *439*, 135678. [[CrossRef](#)]
125. Zhang, X.; Ma, F.; Srinivas, K.; Yu, B.; Chen, X.; Wang, B.; Wang, X.; Liu, D.; Zhang, Z.; He, J.; et al. Fe₃N@N-doped graphene as a lithiophilic interlayer for highly stable lithium metal batteries. *Energy Storage Mater.* **2022**, *45*, 656–666. [[CrossRef](#)]
126. Kim, Y.H.; Lee, G.W.; Choi, Y.J.; Choi, H.S.; Kim, K.B. Mechanically Resilient Graphene Assembly Microspheres with Interlocked N-Doped Graphene Nanostructures Grown In Situ for Highly Stable Lithium Metal Anodes. *Adv. Funct. Mater.* **2022**, *32*, 2113316. [[CrossRef](#)]
127. Zhang, Q.; Wang, C.; Xie, Z.; Zhou, Z. Defective/Doped Graphene-Based Materials as Cathodes for Metal–Air Batteries. *Energy Environ. Mater.* **2022**, *5*, 1103–1116. [[CrossRef](#)]
128. He, S.M.; Huang, C.C.; Liou, J.W.; Woon, W.Y.; Su, C.Y. Spectroscopic and electrical characterizations of low-damage phosphorous-doped graphene via ion implantation. *ACS Appl. Mater. Interfaces* **2019**, *11*, 47289–47298. [[CrossRef](#)]
129. Tung, T.T.; Alotaibi, F.; Nine, M.J.; Silva, R.; Tran, D.N.; Janowska, I.; Losic, D. Engineering of highly conductive and ultra-thin nitrogen-doped graphene films by combined methods of microwave irradiation, ultrasonic spraying and thermal annealing. *Chem. Eng. J.* **2018**, *338*, 764–773. [[CrossRef](#)]
130. Qiu, Y.; Xinfeng, Z.; Shihe, Y. High performance supercapacitors based on highly conductive nitrogen-doped graphene sheets. *Phys. Chem. Chem. Phys.* **2011**, *13*, 12554–12558. [[CrossRef](#)]
131. Al-Aqtash, N.; Al-Tarawneh, K.M.; Tawalbeh, T.; Vasiliev, I. Ab initio study of the interactions between boron and nitrogen dopants in graphene. *J. Appl. Phys.* **2012**, *112*, 034304. [[CrossRef](#)]
132. Lambin, P.; Amara, H.; Ducastelle, F.; Henrard, L. Long-range interactions between substitutional nitrogen dopants in graphene: Electronic properties calculations. *Phys. Rev. B* **2012**, *86*, 045448. [[CrossRef](#)]
133. Abdullah, N.R.; Rashid, H.O.; Tang, C.S.; Manolescu, A.; Gudmundsson, V. Controlling physical properties of bilayer graphene by stacking orientation caused by interaction between B and N dopant atoms. *Mater. Sci. Eng. B* **2022**, *276*, 115554. [[CrossRef](#)]
134. Kim, B.J.; Kim, D.H.; Lee, Y.Y.; Shin, H.W.; Han, G.S.; Hong, J.S.; Mahmood, K.; Ahn, T.K.; Joo, Y.C.; Hong, K.S.; et al. Highly efficient and bending durable perovskite solar cells: Toward a wearable power source. *Energy Environ. Sci.* **2015**, *8*, 916–921. [[CrossRef](#)]
135. Seo, S.W.; Lee, H.S.; Shin, D.H.; Kim, J.H.; Jang, C.W.; Kim, J.M.; Kim, S.; Choi, S.H. Highly-stable and-flexible graphene/(CF₃SO₂)₂NH/graphene transparent conductive electrodes for organic solar cells. *Nanotechnology* **2017**, *28*, 425203. [[CrossRef](#)] [[PubMed](#)]
136. Bullock, J.; Ota, H.; Wang, H.; Xu, Z.; Hettick, M.; Yan, D.; Samundsett, C.; Wan, Y.; Essig, S.; Morales-Masis, M.; et al. Microchannel contacting of crystalline silicon solar cells. *Sci. Rep.* **2017**, *7*, 9085. [[CrossRef](#)]
137. Angmo, D.; Krebs, F.C. Flexible ITO-free polymer solar cells. *J. Appl. Polym. Sci.* **2013**, *129*, 1–14. [[CrossRef](#)]
138. Hecht, D.S.; Liangbing, H.; Glen, I. Emerging transparent electrodes based on thin films of carbon nanotubes, graphene, and metallic nanostructures. *Adv. Mater.* **2011**, *23*, 1482–1513. [[CrossRef](#)]
139. Basarir, F.; Irani, F.S.; Kosemen, A.; Camic, B.T.; Oytun, F.; Tunaboylu, B.; Shin, H.J.; Nam, K.Y.; Choi, H. Recent progresses on solution-processed silver nanowire based transparent conducting electrodes for organic solar cells. *Mater. Today Chem.* **2017**, *3*, 60–72. [[CrossRef](#)]
140. Patel, P.K. Carbon nanotube based nano-composites: Introduction, mechanism and finite element analysis. In *Handbook of Carbon Nanotubes*; Springer International Publishing: Cham, Switzerland, 2022; pp. 1–26.
141. De, S.; Coleman, J.N. Are there fundamental limitations on the sheet resistance and transmittance of thin graphene films? *ACS Nano* **2010**, *4*, 2713–2720. [[CrossRef](#)]

142. Gao, L.; Ren, W.; Zhao, J.; Ma, L.P.; Chen, Z.; Cheng, H.M. Efficient growth of high-quality graphene films on Cu foils by ambient pressure chemical vapor deposition. *Appl. Phys. Lett.* **2010**, *97*, 183109.
143. Bao, W.; Wan, J.; Han, X.; Cai, X.; Zhu, H.; Kim, D.; Ma, D.; Xu, Y.; Munday, J.N.; Drew, H.D.; et al. Approaching the limits of transparency and conductivity in graphitic materials through lithium intercalation. *Nat. Commun.* **2014**, *5*, 4224. [[CrossRef](#)] [[PubMed](#)]
144. Gao, P.; Ding, K.; Wang, Y.; Ruan, K.; Diao, S.; Zhang, Q.; Sun, B.; Jie, J. Crystalline Si/graphene quantum dots heterojunction solar cells. *J. Phys. Chem. C* **2014**, *118*, 5164–5171. [[CrossRef](#)]
145. Chuang, M.-K.; Fang-Chung, C.; Chain-Shu, H. Gold nanoparticle-graphene oxide nanocomposites that enhance the device performance of polymer solar cells. *J. Nanomater.* **2014**, *2014*, 179. [[CrossRef](#)]
146. Uma, K.; Subramani, T.; Syu, H.J.; Lin, T.C.; Lin, C.F. Fabrication of silicon nanowire/poly (3, 4-ethylenedioxythiophene): Poly (styrenesulfonate)-graphene oxide hybrid solar cells. *J. Appl. Phys.* **2015**, *117*, 105102. [[CrossRef](#)]
147. Zhang, X.; Xie, C.; Jie, J.; Zhang, X.; Wu, Y.; Zhang, W. High-efficiency graphene/Si nanoarray Schottky junction solar cells via surface modification and graphene doping. *J. Mater. Chem. A* **2013**, *1*, 6593–6601. [[CrossRef](#)]
148. Li, S.S.; Tu, K.H.; Lin, C.C.; Chen, C.W.; Chhowalla, M. Solution-processable graphene oxide as an efficient hole transport layer in polymer solar cells. *ACS Nano* **2010**, *4*, 3169–3174. [[CrossRef](#)]
149. Liu, J.; Kim, G.H.; Xue, Y.; Kim, J.Y.; Baek, J.B.; Durstock, M.; Dai, L. Graphene oxide nanoribbon as hole extraction layer to enhance efficiency and stability of polymer solar cells. *Adv. Mater.* **2014**, *26*, 786–790. [[CrossRef](#)]
150. Muchuweni, E.; Bice, S.M.; Vincent, O.N. Organic solar cells: Current perspectives on graphene-based materials for electrodes, electron acceptors and interfacial layers. *Int. J. Energy Res.* **2021**, *45*, 6518–6549. [[CrossRef](#)]
151. Guo, B.; Fang, L.; Zhang, B.; Gong, J.R. Graphene doping: A review. *Insciences J.* **2011**, *1*, 80–89. [[CrossRef](#)]
152. Xia, F.; Hugen, Y.; Phaeton, A. The interaction of light and graphene: Basics, devices, and applications. *Proc. IEEE* **2013**, *101*, 1717–1731. [[CrossRef](#)]
153. Pykal, M.; Jurečka, P.; Karlický, F.; Otyepka, M. Modelling of graphene functionalization. *Phys. Chem. Chem. Phys.* **2016**, *18*, 6351–6372. [[CrossRef](#)] [[PubMed](#)]
154. Kakavelakis, G.; Konios, D.; Stratakis, E.; Kymakis, E. Enhancement of the efficiency and stability of organic photovoltaic devices via the addition of a lithium-neutralized graphene oxide electron-transporting layer. *Chem. Mater.* **2014**, *26*, 5988–5993. [[CrossRef](#)]
155. Jariwala, D.; Anchal, S.; Pulickel, M.A. Graphene synthesis and band gap opening. *J. Nanosci. Nanotechnol.* **2011**, *11*, 6621–6641. [[CrossRef](#)]
156. Liu, X.; Wen, Y.; Chen, Z.; Lin, H.; Chen, R.; Cho, K.; Shan, B. Modulation of Dirac points and band-gaps in graphene via periodic fullerene adsorption. *AIP Adv.* **2013**, *3*, 052126. [[CrossRef](#)]
157. Dvorak, M.; William, O.; Zhigang, W. Bandgap opening by patterning graphene. *Sci. Rep.* **2013**, *3*, 2289. [[CrossRef](#)]
158. Soo Park, C.; Zhao, Y.; Lee, J.H.; Whang, D.; Shon, Y.; Song, Y.H.; Jin Lee, C. Tunable bandgap of a single layer graphene doped by the manganese oxide using the electrochemical doping. *Appl. Phys. Lett.* **2013**, *102*, 032106. [[CrossRef](#)]
159. Li, X.; Zhu, H.; Wang, K.; Cao, A.; Wei, J.; Li, C.; Jia, Y.; Li, Z.; Li, X.; Wu, D. Graphene-on-silicon Schottky junction solar cells. *Adv. Mater.* **2010**, *22*, 2743–2748. [[CrossRef](#)]
160. Tsuboi, Y.; Wang, F.; Kozawa, D.; Funahashi, K.; Mouri, S.; Miyauchi, Y.; Takenobu, T.; Matsuda, K. Enhanced photovoltaic performances of graphene/Si solar cells by insertion of a MoS₂ thin film. *Nanoscale* **2015**, *7*, 14476–14482. [[CrossRef](#)]
161. Mohammed, M.; Li, Z.; Cui, J.; Chen, T.P. Junction investigation of graphene/silicon Schottky diodes. *Nanoscale Res. Lett.* **2012**, *7*, 1–6. [[CrossRef](#)]
162. Bari, B.; Lee, J.; Jang, T.; Won, P.; Ko, S.H.; Alamgir, K.; Arshad, M.; Guo, L.J. Simple hydrothermal synthesis of very-long and thin silver nanowires and their application in high quality transparent electrodes. *J. Mater. Chem. A* **2016**, *4*, 11365–11371. [[CrossRef](#)]
163. Xue, Q.; Yao, W.; Liu, J.; Tian, Q.; Liu, L.; Li, M.; Lu, Q.; Peng, R.; Wu, W. Facile synthesis of silver nanowires with different aspect ratios and used as high-performance flexible transparent electrodes. *Nanoscale Res. Lett.* **2017**, *12*, 1–12. [[CrossRef](#)] [[PubMed](#)]
164. Yang, L.; Yu, X.; Hu, W.; Wu, X.; Zhao, Y.; Yang, D. An 8.68% efficiency chemically-doped-free graphene–silicon solar cell using silver nanowires network buried contacts. *ACS Appl. Mater. Interfaces* **2015**, *7*, 4135–4141. [[CrossRef](#)] [[PubMed](#)]
165. Liu, X.; Zhang, X.W.; Meng, J.H.; Yin, Z.G.; Zhang, L.Q.; Wang, H.L.; Wu, J.L. High efficiency Schottky junction solar cells by co-doping of graphene with gold nanoparticles and nitric acid. *Appl. Phys. Lett.* **2015**, *106*, 233901. [[CrossRef](#)]
166. D’Arsié, L.; Esconjauregui, S.; Weatherup, R.S.; Wu, X.; Arter, W.E.; Sugime, H.; Cepek, C.; Robertson, J. Stable, efficient p-type doping of graphene by nitric acid. *RSC Adv.* **2016**, *6*, 113185–113192. [[CrossRef](#)]
167. Kim, J.M.; Kim, S.; Shin, D.H.; Seo, S.W.; Lee, H.S.; Kim, J.H.; Jang, C.W.; Kang, S.S.; Choi, S.H.; Kwak, G.Y.; et al. Si-quantum-dot heterojunction solar cells with 16.2% efficiency achieved by employing doped-graphene transparent conductive electrodes. *Nano Energy* **2018**, *43*, 124–129. [[CrossRef](#)]
168. Aziz, W.J.; Ramizy, A.; Ibrahim, K.; Hassan, Z.; Omar, K. The effect of anti-reflection coating of porous silicon on solar cells efficiency. *Optik* **2011**, *122*, 1462–1465. [[CrossRef](#)]
169. Menna, P.; Di Francia, G.; La Ferrara, V. Porous silicon in solar cells: A review and a description of its application as an AR coating. *Sol. Energy Mater. Sol. Cells* **1995**, *37*, 13–24. [[CrossRef](#)]
170. Miranda, C.R.; Baldan, M.R.; Beloto, A.F.; Ferreira, N.G. Morphological and optical characteristics of porous silicon produced by anodization process in HF-acetonitrile and HF-ethanol solutions. *J. Braz. Chem. Soc.* **2008**, *19*, 769–774. [[CrossRef](#)]

171. Shin, D.H.; Kim, J.H.; Kim, J.H.; Jang, C.W.; Seo, S.W.; Lee, H.S.; Kim, S.; Choi, S.H. Graphene/porous silicon Schottky-junction solar cells. *J. Alloys Compd.* **2017**, *715*, 291–296. [[CrossRef](#)]
172. Jang, C.W.; Kim, J.M.; Kim, J.H.; Shin, D.H.; Kim, S.; Choi, S.H. Degradation reduction and stability enhancement of p-type graphene by RhCl₃ doping. *J. Alloys Compd.* **2015**, *621*, 1–6. [[CrossRef](#)]
173. Kim, J.H.; Shin, D.H.; Lee, H.S.; Jang, C.W.; Kim, J.M.; Seo, S.W.; Kim, S.; Choi, S.H. Enhancement of efficiency in graphene/porous silicon solar cells by co-doping graphene with gold nanoparticles and bis (trifluoromethanesulfonyl)-amide. *J. Mater. Chem. C* **2017**, *5*, 9005–9011. [[CrossRef](#)]
174. Peng, K.; Xu, Y.; Wu, Y.; Yan, Y.; Lee, S.T.; Zhu, J. Aligned single-crystalline Si nanowire arrays for photovoltaic applications. *Small* **2005**, *1*, 1062–1067. [[CrossRef](#)] [[PubMed](#)]
175. Sivakov, V.; Andrä, G.; Gawlik, A.; Berger, A.; Plentz, J.; Falk, F.; Christiansen, S.H. Silicon nanowire-based solar cells on glass: Synthesis, optical properties, and cell parameters. *Nano Lett.* **2009**, *9*, 1549–1554. [[CrossRef](#)] [[PubMed](#)]
176. Pavesi, L.; Dal Negro, L.; Mazzoleni, C.; Franzo, G.; Priolo, D.F. Optical gain in silicon nanocrystals. *Nature* **2000**, *408*, 440–444. [[CrossRef](#)] [[PubMed](#)]
177. Duan, Y.; Kong, J.F.; Shen, W.Z. Raman investigation of silicon nanocrystals: Quantum confinement and laser-induced thermal effects. *J. Raman Spectrosc.* **2012**, *43*, 756–760. [[CrossRef](#)]
178. Minemoto, T.; Masashi, M. Theoretical analysis on effect of band offsets in perovskite solar cells. *Sol. Energy Mater. Sol. Cells* **2015**, *133*, 8–14. [[CrossRef](#)]
179. Bagade, S.S.; Barik, S.B.; Malik, M.M.; Patel, P.K. Impact of band alignment at interfaces in perovskite-based solar cell devices. *Mater. Today Proc.* **2023**, in press. [[CrossRef](#)]
180. Cho, E.C.; Park, S.; Hao, X.; Song, D.; Conibeer, G.; Park, S.C.; Green, M.A. Silicon quantum dot/crystalline silicon solar cells. *Nanotechnology* **2008**, *19*, 245201. [[CrossRef](#)]
181. Park, S.; Cho, E.; Hao, X.; Conibeer, G.; Green, M.A. Study of silicon quantum dot pn or pin junction devices on c-Si substrate. In Proceedings of the 2008 Conference on Optoelectronic and Microelectronic Materials and Devices, Sidney, Australia, 28 July–1 August 2008.
182. Hong, S.H.; Park, J.H.; Shin, D.H.; Kim, C.O.; Choi, S.H.; Kim, K.J. Doping-and size-dependent photovoltaic properties of p-type Si-quantum-dot heterojunction solar cells: Correlation with photoluminescence. *Appl. Phys. Lett.* **2010**, *97*, 072108. [[CrossRef](#)]
183. Hong, S.H.; Kim, Y.S.; Lee, W.; Kim, Y.H.; Song, J.Y.; Jang, J.S.; Park, J.H.; Choi, S.H.; Kim, K.J. Active doping of B in silicon nanostructures and development of a Si quantum dot solar cell. *Nanotechnology* **2011**, *22*, 425203. [[CrossRef](#)]
184. Lee, S.H.; Kwak, G.Y.; Hong, S.; Kim, C.; Kim, S.; Kim, A.; Kim, K.J. Ultraviolet responses of a heterojunction Si quantum dot solar cell. *Nanotechnology* **2016**, *28*, 035402. [[CrossRef](#)] [[PubMed](#)]
185. Shin, D.H.; Jang, C.W.; Lee, H.S.; Seo, S.W.; Kim, S.; Choi, S.H. Graphene/Si solar cells employing triethylenetetramine dopant and polymethylmethacrylate antireflection layer. *Appl. Surf. Sci.* **2018**, *433*, 181–187. [[CrossRef](#)]
186. Park, S.H.; Roy, A.; Beaupré, S.; Cho, S.; Coates, N.; Moon, J.S.; Moses, D.; Leclerc, M.; Lee, K.; Heeger, A.J. Bulk heterojunction solar cells with internal quantum efficiency approaching 100%. *Nat. Photonics* **2009**, *3*, 297–302. [[CrossRef](#)]
187. Chen, F.-C.; Shang-Chieh, C. Nanoscale functional interlayers formed through spontaneous vertical phase separation in polymer photovoltaic devices. *J. Mater. Chem.* **2009**, *19*, 6865–6869. [[CrossRef](#)]
188. Bedeloglu, A.; Demir, A.; Bozkurt, Y.; Sariciftci, N.S. A flexible textile structure based on polymeric photovoltaics using transparent cathode. *Synth. Met.* **2009**, *159*, 2043–2048. [[CrossRef](#)]
189. Galagan, Y.; Rubingh, J.E.J.; Andriessen, R.; Fan, C.C.; Blom, P.W.; Veenstra, S.C.; Kroon, J.M. ITO-free flexible organic solar cells with printed current collecting grids. *Sol. Energy Mater. Sol. Cells* **2011**, *95*, 1339–1343. [[CrossRef](#)]
190. Zhong, Y.; Liu, D.; Zhang, K.; Li, Y.; Sun, M.; Yu, L.; Li, F.; Liu, H.; Yang, R. Modifying the morphology via employing rigid phenyl side chains achieves efficient nonfullerene polymer solar cells. *J. Polym. Sci. Part A Polym. Chem.* **2018**, *56*, 2762–2770. [[CrossRef](#)]
191. Liu, F.; Nunzi, J.M. Air stable hybrid inverted tandem solar cell design. *Appl. Phys. Lett.* **2011**, *99*, 159. [[CrossRef](#)]
192. Hau, S.K.; Yip, H.L.; Jen, A.K.Y. A review on the development of the inverted polymer solar cell architecture. *Polym. Rev.* **2010**, *50*, 474–510. [[CrossRef](#)]
193. Said Karim, S.; Gunnella, R. Efficient method of fabricating polymeric solar cells in multilayered configuration using electrospray. *J. Electron. Mater.* **2020**, *49*, 1794–1800.
194. Hadipour, A.; de Boer, B.; Blom, P.W.M. Organic tandem and multi-junction solar cells. *Adv. Funct. Mater.* **2008**, *18*, 169–181. [[CrossRef](#)]
195. Krishna, K.M.; Muthuvinayagam, M. Graphene nanotechnology for renewable energy systems. In *Graphene: Fabrication, Properties and Applications*; Springer Nature: Singapore, 2023; pp. 167–193.
196. Agnieszka, I.; Chuchmała, A. Perspectives of applied graphene: Polymer solar cells. *Prog. Polym. Sci.* **2012**, *37*, 1805–1828.
197. Ye, Y.; Lun, D. Graphene-based Schottky junction solar cells. *J. Mater. Chem.* **2012**, *22*, 24224–24229. [[CrossRef](#)]
198. Tongay, S.; Schumann, T.; Miao, X.; Appleton, B.R.; Hebard, A.F. Tuning Schottky diodes at the many-layer-graphene/semiconductor interface by doping. *Carbon* **2011**, *49*, 2033–2038. [[CrossRef](#)]
199. Tongay, S.; Schumann, T.; Hebard, A.F. Graphite based Schottky diodes formed on Si, GaAs, and 4H-SiC substrates. *Appl. Phys. Lett.* **2009**, *95*, 222103. [[CrossRef](#)]
200. Tongay, S.; Lemaitre, M.; Schumann, T.; Berke, K.; Appleton, B.R.; Gila, B.; Hebard, A.F. Graphene/GaN Schottky diodes: Stability at elevated temperatures. *Appl. Phys. Lett.* **2011**, *99*, 102102. [[CrossRef](#)]

201. Chen, C.C.; Chang, C.C.; Li, Z.; Levi, A.F.J.; Cronin, S.B. Gate tunable graphene-silicon Ohmic/Schottky contacts. *Appl. Phys. Lett.* **2012**, *101*, 223113. [[CrossRef](#)]
202. Wu, X.; Sprinkle, M.; Li, X.; Ming, F.; Berger, C.; de Heer, W.A. Epitaxial-graphene/graphene-oxide junction: An essential step towards epitaxial graphene electronics. *Phys. Rev. Lett.* **2008**, *101*, 026801. [[CrossRef](#)]
203. Chen, C.C.; Aykol, M.; Chang, C.C.; Levi, A.F.J.; Cronin, S.B. Graphene-silicon Schottky diodes. *Nano Lett.* **2011**, *11*, 1863–1867. [[CrossRef](#)]
204. Ye, Y.; Dai, Y.; Dai, L.; Shi, Z.; Liu, N.; Wang, F.; Fu, L.; Peng, R.; Wen, X.; Chen, Z.; et al. High-Performance Single CdS Nanowire (Nanobelt) Schottky Junction Solar Cells with Au/Graphene Schottky Electrode. *ACS Appl. Mater. Interfaces* **2010**, *2*, 3406–3410. [[CrossRef](#)]
205. Zhang, L.; Fan, L.; Li, Z.; Shi, E.; Li, X.; Li, H.; Ji, C.; Jia, Y.; Wei, J.; Wang, K.; et al. Graphene-CdSe nanobelt solar cells with tunable configurations. *Nano Res.* **2011**, *4*, 891–900. [[CrossRef](#)]
206. Jie, W.; Fengang, Z.; Jianhua, H. Graphene/gallium arsenide-based Schottky junction solar cells. *Appl. Phys. Lett.* **2013**, *103*, 233111. [[CrossRef](#)]
207. Miao, X.; Tongay, S.; Petterson, M.K.; Berke, K.; Rinzler, A.G.; Appleton, B.R.; Hebard, A.F. High efficiency graphene solar cells by chemical doping. *Nano Lett.* **2012**, *12*, 2745–2750. [[CrossRef](#)] [[PubMed](#)]
208. Chen, D.; Zhang, H.; Liu, Y.; Li, J. Graphene and its derivatives for the development of solar cells, photoelectrochemical, and photocatalytic applications. *Energy Environ. Sci.* **2013**, *6*, 1362–1387. [[CrossRef](#)]
209. Wang, H.X.; Wang, Q.; Zhou, K.G.; Zhang, H.L. Graphene in light: Design, synthesis and applications of photo-active graphene and graphene-like materials. *Small* **2013**, *9*, 1266–1283. [[CrossRef](#)] [[PubMed](#)]
210. Tu, W.; Yong, Z.; Zhigang, Z. Versatile graphene-promoting photocatalytic performance of semiconductors: Basic principles, synthesis, solar energy conversion, and environmental applications. *Adv. Funct. Mater.* **2013**, *23*, 4996–5008. [[CrossRef](#)]
211. Zhang, J.; Zhao, F.; Zhang, Z.; Chen, N.; Qu, L. Dimension-tailored functional graphene structures for energy conversion and storage. *Nanoscale* **2013**, *5*, 3112–3126. [[CrossRef](#)]
212. Muchuweni, E.; Bice, S.M.; Vincent, O. Nyamori. Recent advances in graphene-based materials for dye-sensitized solar cell fabrication. *RSC Adv.* **2020**, *10*, 44453–44469. [[CrossRef](#)]
213. Song, J.; Yin, Z.; Yang, Z.; Amaladass, P.; Wu, S.; Ye, J.; Zhao, Y.; Deng, W.Q.; Zhang, H.; Liu, X.W. Enhancement of photogenerated electron transport in dye-sensitized solar cells with introduction of a reduced graphene oxide–TiO₂ junction. *Chem. A Eur. J.* **2011**, *17*, 10832–10837. [[CrossRef](#)]
214. Tang, Y.B.; Lee, C.S.; Xu, J.; Liu, Z.T.; Chen, Z.H.; He, Z.; Cao, Y.L.; Yuan, G.; Song, H.; Chen, L.; et al. Incorporation of graphenes in nanostructured TiO₂ films via molecular grafting for dye-sensitized solar cell application. *ACS Nano* **2010**, *4*, 3482–3488. [[CrossRef](#)]
215. Bell, N.J.; Ng, Y.H.; Du, A.; Coster, H.; Smith, S.C.; Amal, R. Understanding the enhancement in photoelectrochemical properties of photocatalytically prepared TiO₂-reduced graphene oxide composite. *J. Phys. Chem. C* **2011**, *115*, 6004–6009. [[CrossRef](#)]
216. Neo, C.Y.; Jianyong, O. Graphene oxide as auxiliary binder for TiO₂ nanoparticle coating to more effectively fabricate dye-sensitized solar cells. *J. Power Sources* **2013**, *222*, 161–168. [[CrossRef](#)]
217. Tang, B.; Guoxin, H. Two kinds of graphene-based composites for photoanode applying in dye-sensitized solar cell. *J. Power Sources* **2012**, *220*, 95–102. [[CrossRef](#)]
218. Yang, N.; Zhai, J.; Wang, D.; Chen, Y.; Jiang, L. Two-dimensional graphene bridges enhanced photoinduced charge transport in dye-sensitized solar cells. *ACS Nano* **2010**, *4*, 887–894. [[CrossRef](#)]
219. Chen, T.; Hu, W.; Song, J.; Guai, G.H.; Li, C.M. Interface functionalization of photoelectrodes with graphene for high performance dye-sensitized solar cells. *Adv. Funct. Mater.* **2012**, *22*, 5245–5250. [[CrossRef](#)]
220. Kim, H.-N.; Haemin, Y.; Jun, H.M. Graphene-embedded 3D TiO₂ inverse opal electrodes for highly efficient dye-sensitized solar cells: Morphological characteristics and photocurrent enhancement. *Nanoscale* **2013**, *5*, 4200–4204. [[CrossRef](#)]
221. Tang, B.; Hu, G.; Gao, H.; Shi, Z. Three-dimensional graphene network assisted high performance dye sensitized solar cells. *J. Power Sources* **2013**, *234*, 60–68. [[CrossRef](#)]
222. Nair, R.R.; Blake, P.; Grigorenko, A.N.; Novoselov, K.S.; Booth, T.J.; Stauber, T.; Peres, N.M.; Geim, A.K. Fine structure constant defines visual transparency of graphene. *Science* **2008**, *320*, 1308. [[CrossRef](#)]
223. Grätzel, M. Photoelectrochemical cells. *Nature* **2001**, *414*, 338–344. [[CrossRef](#)]
224. Grätzel, M. Conversion of sunlight to electric power by nanocrystalline dye-sensitized solar cells. *J. Photochem. Photobiol. A Chem.* **2004**, *164*, 3–14. [[CrossRef](#)]
225. Trancik, J.E.; Scott, C.B.; Hone, J. Transparent and catalytic carbon nanotube films. *Nano Lett.* **2008**, *8*, 982–987. [[CrossRef](#)] [[PubMed](#)]
226. Li, G.R.; Wang, F.; Jiang, Q.W.; Gao, X.P.; Shen, P.W. Carbon nanotubes with titanium nitride as a low-cost counter-electrode material for dye-sensitized solar cells. *Angew. Chem. Int. Ed.* **2010**, *49*, 3653–3656. [[CrossRef](#)] [[PubMed](#)]
227. Wang, M.; Anghel, A.M.; Marsan, B.; Cevey Ha, N.L.; Pootrakulchote, N.; Zakeeruddin, S.M.; Grätzel, M. CoS supersedes Pt as efficient electrocatalyst for triiodide reduction in dye-sensitized solar cells. *J. Am. Chem. Soc.* **2009**, *131*, 15976–15977. [[CrossRef](#)]
228. Barik, S.B.; Patidar, P.; Bagade, S.S.; Kumar, A.; Nayak, R.K.; Patel, P.K. Recent progress in reinforcement of nanofillers in epoxy-based nanocomposites. *Mater. Today Proc.* **2023**; *in press*.

229. Chavez-Valdez, A.R.B.A.; Shaffer, M.S.; Boccaccini, A.R. Applications of graphene electrophoretic deposition. A review. *J. Phys. Chem. B* **2013**, *117*, 1502–1515. [[CrossRef](#)]
230. Acik, M.; Lee, G.; Mattevi, C.; Chhowalla, M.; Cho, K.; Chabal, Y.J. Unusual infrared-absorption mechanism in thermally reduced graphene oxide. *Nat. Mater.* **2010**, *9*, 840–845. [[CrossRef](#)] [[PubMed](#)]
231. Hasin, P.; Mario, A. Alpuche-Aviles, and Yiyang Wu. Electrocatalytic activity of graphene multilayers toward I⁻/I₃⁻: Effect of preparation conditions and polyelectrolyte modification. *J. Phys. Chem. C* **2010**, *114*, 15857–15861. [[CrossRef](#)]
232. Mueller, M.L.; Yan, X.; McGuire, J.A.; Li, L.S. Triplet states and electronic relaxation in photoexcited graphene quantum dots. *Nano Lett.* **2010**, *10*, 2679–2682. [[CrossRef](#)]
233. Zhu, S.; Song, Y.; Zhao, X.; Shao, J.; Zhang, J.; Yang, B. The photoluminescence mechanism in carbon dots (graphene quantum dots, carbon nanodots, and polymer dots): Current state and future perspective. *Nano Res.* **2015**, *8*, 355–381. [[CrossRef](#)]
234. Lee, E.; Jaehoon, R.; Jyongsik, J. Fabrication of graphene quantum dots via size-selective precipitation and their application in upconversion-based DSSCs. *Chem. Commun.* **2013**, *49*, 9995–9997. [[CrossRef](#)]
235. Guo, X.; Ganhua, L.; Junhong, C. Graphene-based materials for photoanodes in dye-sensitized solar cells. *Front. Energy Res.* **2015**, *3*, 50. [[CrossRef](#)]
236. Madhavan, A.A.; Kalluri, S.; Chacko, D.K.; Arun, T.A.; Nagarajan, S.; Subramanian, K.R.; Nair, A.S.; Nair, S.V.; Balakrishnan, A. Electrical and optical properties of electrospun TiO₂-graphene composite nanofibers and its application as DSSC photo-anodes. *RSC Adv.* **2012**, *2*, 13032–13037. [[CrossRef](#)]
237. Kamat, P.V. Quantum dot solar cells. Semiconductor nanocrystals as light harvesters. *J. Phys. Chem. C* **2008**, *112*, 18737–18753. [[CrossRef](#)]
238. Smith, A.M.; Shuming, N. Semiconductor nanocrystals: Structure, properties, and band gap engineering. *Acc. Chem. Res.* **2010**, *43*, 190–200. [[CrossRef](#)] [[PubMed](#)]
239. Jha, D.; Dixit, A.; Sushrutha, A.; Patel, P.K. Optical simulations and optimization of highly efficient GaAs based quantum dot solar cell. *Opt. Commun.* **2022**, *523*, 128717. [[CrossRef](#)]
240. Tisdale, W.A.; Williams, K.J.; Timp, B.A.; Norris, D.J.; Aydil, E.S.; Zhu, X.Y. Hot-electron transfer from semiconductor nanocrystals. *Science* **2010**, *328*, 1543–1547. [[CrossRef](#)]
241. Semonin, O.E.; Luther, J.M.; Choi, S.; Chen, H.Y.; Gao, J.; Nozik, A.J.; Beard, M.C. Peak external photocurrent quantum efficiency exceeding 100% via MEG in a quantum dot solar cell. *Science* **2011**, *334*, 1530–1533. [[CrossRef](#)]
242. Tachan, Z.; Hod, I.; Shalom, M.; Grinis, L.; Zaban, A. The importance of the TiO₂/quantum dots interface in the recombination processes of quantum dot sensitized solar cells. *Phys. Chem. Chem. Phys.* **2013**, *15*, 3841–3845. [[CrossRef](#)]
243. Lee, J.W.; Son, D.Y.; Ahn, T.K.; Shin, H.W.; Kim, I.Y.; Hwang, S.J.; Ko, M.J.; Sul, S.; Han, H.; Park, N.G. Quantum-dot-sensitized solar cell with unprecedentedly high photocurrent. *Sci. Rep.* **2013**, *3*, 1050. [[CrossRef](#)]
244. Sudhagar, P.; Asokan, K.; Ito, E.; Kang, Y.S. N-Ion-implanted TiO₂ photoanodes in quantum dot-sensitized solar cells. *Nanoscale* **2012**, *4*, 2416–2422. [[CrossRef](#)]
245. Sudhagar, P.; Song, T.; Jeon, Y.; Mora-Seró, I.; Fabregat-Santiago, F.; Bisquert, J.; Kang, Y.S.; Paik, U. Three dimensional-TiO₂ nanotube array photoanode architectures assembled on a thin hollow nanofibrous backbone and their performance in quantum dot-sensitized solar cells. *ChemComm* **2013**, *49*, 2810–2812.
246. de la Fuente, M.S.; Sánchez, R.S.; González-Pedro, V.; Boix, P.P.; Mhaisalkar, S.G.; Rincon, M.E.; Bisquert, J.; Mora-Sero, I. Effect of organic and inorganic passivation in quantum-dot-sensitized solar cells. *J. Phys. Chem. Lett.* **2013**, *4*, 1519–1525. [[CrossRef](#)] [[PubMed](#)]
247. Braga, A.; Giménez, S.; Concina, I.; Vomiero, A.; Mora-Seró, I. Panchromatic sensitized solar cells based on metal sulfide quantum dots grown directly on nanostructured TiO₂ electrodes. *J. Phys. Chem. Lett.* **2011**, *2*, 454–460. [[CrossRef](#)]
248. Sudhagar, P.; Ramasamy, E.; Cho, W.H.; Lee, J.; Kang, Y.S. Robust mesocellular carbon foam counter electrode for quantum-dot sensitized solar cells. *Electrochem. Commun.* **2011**, *13*, 34–37. [[CrossRef](#)]
249. Guo, C.X.; Yang, H.B.; Sheng, Z.M.; Lu, Z.S.; Song, Q.L.; Li, C.M. Layered graphene/quantum dots for photovoltaic devices. *Angew. Chem. Int. Ed.* **2010**, *49*, 3014–3017. [[CrossRef](#)] [[PubMed](#)]
250. Sun, S.; Gao, L.; Liu, Y.; Sun, J. Assembly of CdSe nanoparticles on graphene for low-temperature fabrication of quantum dot sensitized solar cell. *Appl. Phys. Lett.* **2011**, *98*, 093112. [[CrossRef](#)]
251. Diao, S.; Zhang, X.; Shao, Z.; Ding, K.; Jie, J.; Zhang, X. 12.35% efficient graphene quantum dots/silicon heterojunction solar cells using graphene transparent electrode. *Nano Energy* **2017**, *31*, 359–366. [[CrossRef](#)]
252. Lightcap, I.V.; Prashant, V.K. Fortification of CdSe quantum dots with graphene oxide. Excited state interactions and light energy conversion. *J. Am. Chem. Soc.* **2012**, *134*, 7109–7116. [[CrossRef](#)]
253. Rummeli, M.H.; Rocha, C.G.; Ortmann, F.; Ibrahim, I.; Sevincli, H.; Boerrnert, F.; Kunstmann, J.; Bachmatiuk, A.; Poetschke, M.; Shiraishi, M.; et al. Graphene: Piecing it together. *Adv. Mater.* **2011**, *23*, 4471–4490. [[CrossRef](#)]
254. Geim, A.K.; Grigorieva, I.V. Van der Waals heterostructures. *Nature* **2013**, *499*, 419–425. [[CrossRef](#)]
255. Hong, Y.J.; Yang, J.W.; Lee, W.H.; Ruoff, R.S.; Kim, K.S.; Fukui, T. Van der Waals epitaxial double heterostructure: InAs/single-layer graphene/InAs. *Adv. Mater.* **2013**, *25*, 6847–6853. [[CrossRef](#)]
256. Dröscher, S.; Roulleau, P.; Molitor, F.; Studerus, P.; Stampfer, C.; Ensslin, K.; Ihn, T. Quantum capacitance and density of states of graphene. *Appl. Phys. Lett.* **2010**, *96*, 152104. [[CrossRef](#)]
257. Dutta, M.; Sarkar, S.; Ghosh, T.; Basak, D. ZnO/graphene quantum dot solid-state solar cell. *J. Phys. Chem. C* **2012**, *116*, 20127–20131. [[CrossRef](#)]

258. Behura, S.K.; Nayak, S.; Mukhopadhyay, I.; Jani, O. Junction characteristics of chemically-derived graphene/p-Si heterojunction solar cell. *Carbon* **2014**, *67*, 766–774. [[CrossRef](#)]
259. Yin, Z.; Zhu, J.; He, Q.; Cao, X.; Tan, C.; Chen, H.; Yan, Q.; Zhang, H. Graphene-based materials for solar cell applications. *Adv. Energy Mater.* **2014**, *4*, 1300574. [[CrossRef](#)]
260. Wang, P.; Li, X.; Xu, Z.; Wu, Z.; Zhang, S.; Xu, W.; Zhong, H.; Chen, H.; Li, E.; Luo, J.; et al. Tunable graphene/indium phosphide heterostructure solar cells. *Nano Energy* **2015**, *13*, 509–517. [[CrossRef](#)]
261. Song, Y.; Li, X.; Mackin, C.; Zhang, X.; Fang, W.; Palacios, T.; Zhu, H.; Kong, J. Role of interfacial oxide in high-efficiency graphene–silicon Schottky barrier solar cells. *Nano Lett.* **2015**, *15*, 2104–2110. [[CrossRef](#)]
262. Li, X.; Chen, W.; Zhang, S.; Wu, Z.; Wang, P.; Xu, Z.; Chen, H.; Yin, W.; Zhong, H.; Lin, S. 18.5% efficient graphene/GaAs van der Waals heterostructure solar cell. *Nano Energy* **2015**, *16*, 310–319. [[CrossRef](#)]
263. Xia, Y.; Zhu, M.; Qin, L.; Zhao, C.; Hong, D.; Tian, Y.; Yan, W.; Jin, Z. Organic-inorganic hybrid quasi-2D perovskites incorporated with fluorinated additives for efficient and stable four-terminal tandem solar cells. *Energy Mater.* **2023**, *3*, 300004. [[CrossRef](#)]
264. Chen, Y.; Lin, W.C.; Liu, J.; Dai, L. Graphene oxide-based carbon interconnecting layer for polymer tandem solar cells. *Nano Lett.* **2014**, *14*, 1467–1471. [[CrossRef](#)]
265. Tung, V.C.; Jaemyung, K.; Jiaying, H. Graphene oxide: Single-walled carbon nanotube-based interfacial layer for all-solution-processed multijunction solar cells in both regular and inverted geometries. *Adv. Energy Mater.* **2012**, *2*, 299–303. [[CrossRef](#)]
266. Jeon, N.J.; Noh, J.H.; Yang, W.S.; Kim, Y.C.; Ryu, S.; Seo, J.; Seok, S.I. Compositional engineering of perovskite materials for high-performance solar cells. *Nature* **2015**, *517*, 476–480. [[CrossRef](#)] [[PubMed](#)]
267. Park, N.-G. Perovskite solar cells: An emerging photovoltaic technology. *Mater. Today* **2015**, *18*, 65–72. [[CrossRef](#)]
268. Wessendorf, C.D.; Hanisch, J.; Müller, D.; Ahlswede, E. CdS as Electron Transport Layer for Low-Hysteresis Perovskite Solar Cells. *Sol. RRL* **2018**, *2*, 1800056. [[CrossRef](#)]
269. Dehghan, M.; Behjat, A. Deposition of zinc oxide as an electron transport layer in planar perovskite solar cells by spray and SILAR methods comparable with spin coating. *RSC Adv.* **2019**, *9*, 20917–20924. [[CrossRef](#)] [[PubMed](#)]
270. Mahapatra, B.; Rangam, V.K.; Piyush, K.P. Design and optimization of CuSCN/CH₃NH₃PbI₃/TiO₂ perovskite solar cell for efficient performance. *Opt. Commun.* **2022**, *504*, 127496. [[CrossRef](#)]
271. Krishna, R.V.; Brahmadutta, M.; Piyush, K.P. Effect of electrical parameters on lead-based perovskite solar cell for high-efficiency performance. *Opt. Quantum Electron.* **2022**, *54*, 513. [[CrossRef](#)]
272. Krishna, R.V.; Laxmi, L.; Mahapatra, B.; Patel, P.K. Device simulation of CH₃NH₃PbI₃ perovskite solar cell with high efficiency. In Proceedings of the 5th National e-Conference on Advanced Materials and Radiation Physics, Longowal, India, 9–11 November 2021; Volume 2352.
273. Liang, J.; Wu, T.; Wang, Z.; Yu, Y.; Hu, L.; Li, H.; Zhang, X.; Zhu, X.; Zhao, Y. Accelerating perovskite materials discovery and correlated energy applications through artificial intelligence. *Energy Mater* **2022**, *2*, 200016. [[CrossRef](#)]
274. Zhang, J.; Fan, J.; Cheng, B.; Yu, J.; Ho, W. Graphene-based materials in planar perovskite solar cells. *Sol. RRL* **2020**, *4*, 2000502. [[CrossRef](#)]
275. Kuang, C.; Tang, G.; Jiu, T.; Yang, H.; Liu, H.; Li, B.; Luo, W.; Li, X.; Zhang, W.; Lu, F.; et al. Highly efficient electron transport obtained by doping PCBM with graphdiyne in planar-heterojunction perovskite solar cells. *Nano Lett.* **2015**, *15*, 2756–2762. [[CrossRef](#)]
276. Wang, J.T.W.; Ball, J.M.; Barea, E.M.; Abate, A.; Alexander-Webber, J.A.; Huang, J.; Saliba, M.; Mora-Sero, I.; Bisquert, J.; Snaith, H.J.; et al. Low-temperature processed electron collection layers of graphene/TiO₂ nanocomposites in thin film perovskite solar cells. *Nano Lett.* **2014**, *14*, 724–730. [[CrossRef](#)]
277. Zhu, Z.; Ma, J.; Wang, Z.; Mu, C.; Fan, Z.; Du, L.; Bai, Y.; Fan, L.; Yan, H.; Phillips, D.L.; et al. Efficiency enhancement of perovskite solar cells through fast electron extraction: The role of graphene quantum dots. *J. Am. Chem. Soc.* **2014**, *136*, 3760–3763. [[CrossRef](#)] [[PubMed](#)]
278. Wu, Z.; Bai, S.; Xiang, J.; Yuan, Z.; Yang, Y.; Cui, W.; Gao, X.; Liu, Z.; Jin, Y.; Sun, B. Efficient planar heterojunction perovskite solar cells employing graphene oxide as hole conductor. *Nanoscale* **2014**, *6*, 10505–10510. [[CrossRef](#)] [[PubMed](#)]
279. Yeo, J.S.; Kang, R.; Lee, S.; Jeon, Y.J.; Myoung, N.; Lee, C.L.; Kim, D.Y.; Yun, J.M.; Seo, Y.H.; Kim, S.S.; et al. Highly efficient and stable planar perovskite solar cells with reduced graphene oxide nanosheets as electrode interlayer. *Nano Energy* **2015**, *12*, 96–104. [[CrossRef](#)]
280. Li, W.; Dong, H.; Guo, X.; Li, N.; Li, J.; Niu, G.; Wang, L. Graphene oxide as dual functional interface modifier for improving wettability and retarding recombination in hybrid perovskite solar cells. *J. Mater. Chem. A* **2014**, *2*, 20105–20111. [[CrossRef](#)]
281. Yan, K.; Wei, Z.; Li, J.; Chen, H.; Yi, Y.; Zheng, X.; Long, X.; Wang, Z.; Wang, J.; Xu, J.; et al. High-performance graphene-based hole conductor-free perovskite solar cells: Schottky junction enhanced hole extraction and electron blocking. *Small* **2015**, *11*, 2269–2274. [[CrossRef](#)]
282. Im, J.H.; Jang, I.H.; Pellet, N.; Grätzel, M.; Park, N.G. Growth of CH₃NH₃PbI₃ cuboids with controlled size for high-efficiency perovskite solar cells. *Nat. Nanotechnol.* **2014**, *9*, 927–932. [[CrossRef](#)]
283. Zhou, H.P.; You, J.B.; Liu, Y.S.; Yang, Y. Interface engineering of highly efficient perovskite solar cells. *Science* **2014**, *345*, 542–546. [[CrossRef](#)]

284. Yun, J.M.; Yeo, J.S.; Kim, J.; Jeong, H.G.; Kim, D.Y.; Noh, Y.J.; Kim, S.S.; Ku, B.C.; Na, S.I. Solution-processable reduced graphene oxide as a novel alternative to PEDOT: PSS hole transport layers for highly efficient and stable polymer solar cells. *Adv. Mater.* **2011**, *23*, 4923–4928. [[CrossRef](#)]
285. Xie, C.; Zhang, X.; Ruan, K.; Shao, Z.; Dhaliwal, S.S.; Wang, L.; Zhang, Q.; Zhang, X.; Jie, J. High-efficiency, air stable graphene/Si micro-hole array Schottky junction solar cells. *J. Mater. Chem. A* **2013**, *1*, 15348–15354. [[CrossRef](#)]
286. Shi, E.; Li, H.; Yang, L.; Zhang, L.; Li, Z.; Li, P.; Shang, Y.; Wu, S.; Li, X.; Wei, J.; et al. Colloidal antireflection coating improves graphene–silicon solar cells. *Nano Lett.* **2013**, *13*, 1776–1781. [[CrossRef](#)]
287. Brus, V.V.; Gluba, M.A.; Zhang, X.; Hinrichs, K.; Rappich, J.; Nickel, N.H. Stability of graphene–silicon heterostructure solar cells. *Phys. Status Solidi* **2014**, *211*, 843–847. [[CrossRef](#)]
288. Lancellotti, L.; Bobeico, E.; Capasso, A.; Della Noce, M.; Dikonimos, T.; Lisi, N.; Delli Veneri, P. Effects of HNO₃ molecular doping in graphene/Si Schottky barrier solar cells. In Proceedings of the Fotonica AEIT Italian Conference on Photonics Technologies, Naples, Italy, 12–14 May 2014.
289. Yang, H.B.; Dong, Y.Q.; Wang, X.; Khoo, S.Y.; Liu, B. Cesium carbonate functionalized graphene quantum dots as stable electron-selective layer for improvement of inverted polymer solar cells. *ACS Appl. Mater. Interfaces* **2014**, *6*, 1092–1099. [[CrossRef](#)] [[PubMed](#)]
290. Wang, Q.; Jin, Z.; Chen, D.; Bai, D.; Bian, H.; Sun, J.; Zhu, G.; Wang, G.; Liu, S. 2018. μ -Graphene Crosslinked CsPbI₃ Quantum Dots for High Efficiency Solar Cells with Much Improved Stability. *Adv. Energy Mater.* **2018**, *8*, 1800007. [[CrossRef](#)]
291. Jeon, Y.J.; Yun, J.M.; Kim, D.Y.; Na, S.I.; Kim, S.S. High-performance polymer solar cells with moderately reduced graphene oxide as an efficient hole transporting layer. *Sol. Energy Mater. Sol. Cells* **2012**, *105*, 96–102. [[CrossRef](#)]
292. Kwon, K.C.; Dong, W.J.; Jung, G.H.; Ham, J.; Lee, J.L.; Kim, S.Y. Extension of stability in organic photovoltaic cells using UV/ozone-treated graphene sheets. *Sol. Energy Mater. Sol. Cells* **2013**, *109*, 148–154. [[CrossRef](#)]
293. Chen, L.; Du, D.; Sun, K.; Hou, J.; Ouyang, J. Improved efficiency and stability of polymer solar cells utilizing two-dimensional reduced graphene oxide: Graphene oxide nanocomposites as hole-collection material. *ACS Appl. Mater. Interfaces* **2014**, *6*, 22334–22342. [[CrossRef](#)]
294. Gong, K.; Hu, J.; Cui, N.; Xue, Y.; Li, L.; Long, G.; Lin, S. The roles of graphene and its derivatives in perovskite solar cells: A review. *Mater. Des.* **2021**, *211*, 110170. [[CrossRef](#)]
295. Yan, J.; Brian, R.S. Third-generation solar cells: A review and comparison of polymer: Fullerene, hybrid polymer and perovskite solar cells. *RSC Adv.* **2014**, *4*, 43286–43314. [[CrossRef](#)]
296. Safie, N.E.; Azam, M.A.; Aziz, M.F.; Ismail, M. Recent progress of graphene-based materials for efficient charge transfer and device performance stability in perovskite solar cells. *Int. J. Energy Res.* **2021**, *45*, 1347–1374. [[CrossRef](#)]
297. Ndlovu, S.; Ollengo, M.A.; Muchuweni, E.; Nyamori, V.O. Current advances in perovskite oxides supported on graphene-based materials as interfacial layers of perovskite solar cells. *Crit. Rev. Solid State Mater. Sci.* **2023**, *48*, 112–131. [[CrossRef](#)]
298. Wang, D.H.; Kim, J.K.; Seo, J.H.; Park, I.; Hong, B.H.; Park, J.H.; Heeger, A.J. Transferable graphene oxide by stamping nanotechnology: Electron-transport layer for efficient bulk-heterojunction solar cells. *Angew. Chem.* **2013**, *52*, 2874–2880. [[CrossRef](#)] [[PubMed](#)]
299. Jung, H.S.; Nam-Gyu, P. Perovskite solar cells: From materials to devices. *Small* **2015**, *11*, 10–25. [[CrossRef](#)] [[PubMed](#)]
300. Sung, H.; Ahn, N.; Jang, M.S.; Lee, J.K.; Yoon, H.; Park, N.G.; Choi, M. Transparent conductive oxide-free graphene-based perovskite solar cells with over 17% efficiency. *Adv. Energy Mater.* **2016**, *6*, 1501873. [[CrossRef](#)]
301. Li, Y.; Meng, L.; Yang, Y.; Xu, G.; Hong, Z.; Chen, Q.; You, J.; Li, G.; Yang, Y.; Li, Y. High-efficiency robust perovskite solar cells on ultrathin flexible substrates. *Nat. Commun.* **2016**, *7*, 10214. [[CrossRef](#)] [[PubMed](#)]
302. Yoon, J.; Sung, H.; Lee, G.; Cho, W.; Ahn, N.; Jung, H.S.; Choi, M. Superflexible, high-efficiency perovskite solar cells utilizing graphene electrodes: Towards future foldable power sources. *Energy Environ. Sci.* **2017**, *10*, 337–345. [[CrossRef](#)]
303. Hu, X.; Jiang, H.; Li, J.; Ma, J.; Yang, D.; Liu, Z.; Gao, F.; Liu, S.F. Air and thermally stable perovskite solar cells with CVD-graphene as the blocking layer. *Nanoscale* **2017**, *9*, 8274–8280. [[CrossRef](#)]
304. Luo, Q.; Zhang, Y.; Liu, C.; Li, J.; Wang, N.; Lin, H. Iodide-reduced graphene oxide with dopant-free spiro-OMeTAD for ambient stable and high-efficiency perovskite solar cells. *J. Mater. Chem. A* **2015**, *3*, 15996–16004. [[CrossRef](#)]
305. Bi, E.; Chen, H.; Xie, F.; Wu, Y.; Chen, W.; Su, Y.; Islam, A.; Grätzel, M.; Yang, X.; Han, L. Diffusion engineering of ions and charge carriers for stable efficient perovskite solar cells. *Nat. Commun.* **2017**, *8*, 15330. [[CrossRef](#)]
306. Kim, G.H.; Jang, H.; Yoon, Y.J.; Jeong, J.; Park, S.Y.; Walker, B.; Jeon, I.Y.; Jo, Y.; Yoon, H.; Kim, M.; et al. Fluorine functionalized graphene nano platelets for highly stable inverted perovskite solar cells. *Nano Lett.* **2017**, *17*, 6385–6390. [[CrossRef](#)]
307. Niazi, Z.; Hagfeldt, A.; Goharshadi, E.K. The recent progress on the use of graphene-based nanomaterials in perovskite solar cells. *J. Mater. Chem. A* **2023**, *11*, 6659–6687. [[CrossRef](#)]
308. Katariya, A.; Mahapatra, B.; Patel, P.K.; Rani, J. Optimization of ETM and HTM layer on NFA based BHJ-organic solar cell for high efficiency performance. *Optik* **2021**, *245*, 167717. [[CrossRef](#)]
309. Qi, Q.; Ke, H.; Ye, L. Ternary organic solar cells featuring polythiophene. *Energy Mater.* **2022**, *2*, 200035. [[CrossRef](#)]
310. Velasco Davoise, L.; Díez-Pascual, A.M.; Peña Capilla, R. Application of graphene-related materials in organic solar cells. *Materials* **2022**, *15*, 1171. [[CrossRef](#)] [[PubMed](#)]
311. Park, H.; Brown, P.R.; Bulovic, V.; Kong, J. Graphene as transparent conducting electrodes in organic photovoltaics: Studies in graphene morphology, hole transporting layers, and counter electrodes. *Nano Lett.* **2012**, *12*, 133–140. [[CrossRef](#)] [[PubMed](#)]

312. Cox, M.; Gorodetsky, A.; Kim, B.; Kim, K.S.; Jia, Z.; Kim, P.; Nuckolls, C.; Kymissis, I. Single-layer graphene cathodes for organic photovoltaics. *Appl. Phys. Lett.* **2011**, *98*, 67. [[CrossRef](#)]
313. Fu, F.; Feurer, T.; Jäger, T.; Avancini, E.; Bissig, B.; Yoon, S.; Buecheler, S.; Tiwari, A.N. Low-temperature-processed efficient semi-transparent planar perovskite solar cells for bifacial and tandem applications. *Nat. Commun.* **2015**, *6*, 8932. [[CrossRef](#)]
314. Kanda, H.; Uzum, A.; Baranwal, A.K.; Peiris, T.N.; Umeyama, T.; Imahori, H.; Segawa, H.; Miyasaka, T.; Ito, S. Analysis of sputtering damage on I–V curves for perovskite solar cells and simulation with reversed diode model. *J. Phys. Chem. C* **2016**, *120*, 28441–28447. [[CrossRef](#)]
315. Kang, R.; Oh, S.H.; Na, S.I.; Kim, T.S.; Kim, D.Y. Investigation into the effect of post-annealing on inverted polymer solar cells. *Sol. Energy Mater. Sol. Cells* **2014**, *120*, 131–135. [[CrossRef](#)]
316. Song, Y.; Chang, S.; Gradecak, S.; Kong, J. Visibly-transparent organic solar cells on flexible substrates with all-graphene electrodes. *Adv. Energy Mater.* **2016**, *6*, 1600847. [[CrossRef](#)]
317. Liu, Z.; Jinhua, L.; Feng, Y. Package-free flexible organic solar cells with graphene top electrodes. *Adv. Mater.* **2013**, *25*, 4296–4301. [[CrossRef](#)]
318. Wang, Y.; Chen, X.; Zhong, Y.; Zhu, F.; Loh, K.P. Large area, continuous, few-layered graphene as anodes in organic photovoltaic devices. *Appl. Phys. Lett.* **2009**, *95*, 209. [[CrossRef](#)]
319. Cattin, L.; Dahou, F.; Lare, Y.; Morsli, M.; Tricot, R.; Houari, S.; Mokrani, A.; Jondo, K.; Khelil, A.; Napo, K.; et al. MoO₃ surface passivation of the transparent anode in organic solar cells using ultrathin films. *J. Appl. Phys.* **2009**, *105*, 034507. [[CrossRef](#)]
320. Park, H.; Howden, R.M.; Barr, M.C.; Bulovic, V.; Gleason, K.; Kong, J. Organic solar cells with graphene electrodes and vapor printed poly(3, 4-ethylenedioxythiophene) as the hole transporting layers. *ACS Nano* **2012**, *6*, 6370–6377. [[CrossRef](#)] [[PubMed](#)]
321. Xu, B.; Gopalan, S.A.; Gopalan, A.I.; Muthuchamy, N.; Lee, K.P.; Lee, J.S.; Jiang, Y.; Lee, S.W.; Kim, S.W.; Kim, J.S.; et al. Functional solid additive modified PEDOT: PSS as an anode buffer layer for enhanced photovoltaic performance and stability in polymer solar cells. *Sci. Rep.* **2017**, *7*, 45079. [[CrossRef](#)] [[PubMed](#)]
322. Rafique, S.; Abdullah, S.M.; Shahid, M.M.; Ansari, M.O.; Sulaiman, K. Significantly improved photovoltaic performance in polymer bulk heterojunction solar cells with graphene oxide/PEDOT: PSS double decked hole transport layer. *Sci. Rep.* **2017**, *7*, 39555. [[CrossRef](#)]
323. Kyaw, A.K.K.; Sun, X.W.; Jiang, C.Y.; Lo, G.Q.; Zhao, D.W.; Kwong, D.L. An inverted organic solar cell employing a sol-gel derived ZnO electron selective layer and thermal evaporated MoO₃ hole selective layer. *Appl. Phys. Lett.* **2008**, *93*, 221107. [[CrossRef](#)]
324. Barkat, L.; Hssein, M.; El Jouad, Z.; Cattin, L.; Louarn, G.; Stephant, N.; Khelil, A.; Ghamnia, M.; Addou, M.; Morsli, M.; et al. Efficient hole-transporting layer MoO₃: CuI deposited by co-evaporation in organic photovoltaic cells. *Phys. Status Solidi* **2017**, *214*, 1600433. [[CrossRef](#)]
325. Bao, X.; Zhu, Q.; Wang, T.; Guo, J.; Yang, C.; Yu, D.; Wang, N.; Chen, W.; Yang, R. Simple O₂ plasma-processed V₂O₅ as an anode buffer layer for high-performance polymer solar cells. *ACS Appl. Mater. Interfaces* **2015**, *7*, 7613–7618. [[CrossRef](#)]
326. Hu, L.; Peng, J.; Wang, W.; Xia, Z.; Yuan, J.; Lu, J.; Huang, X.; Ma, W.; Song, H.; Chen, W.; et al. Sequential deposition of CH₃NH₃PbI₃ on planar NiO film for efficient planar perovskite solar cells. *ACS Photonics* **2014**, *1*, 547–553. [[CrossRef](#)]
327. Zhu, Z.; Bai, Y.; Zhang, T.; Liu, Z.; Long, X.; Wei, Z.; Wang, Z.; Zhang, L.; Wang, J.; Yan, F.; et al. High-performance hole-extraction layer of sol-gel-processed NiO nanocrystals for inverted planar perovskite solar cells. *Angew. Chem. Int. Ed.* **2014**, *53*, 12571–12575.
328. Kim, J.; Lee, H.; Lee, S.J.; Da Silva, W.J.; bin Mohd Yusoff, A.R.; Jang, J. Graphene oxide grafted polyethylenimine electron transport materials for highly efficient organic devices. *J. Mater. Chem. A* **2015**, *3*, 22035–22042. [[CrossRef](#)]
329. Cheng, X.; Long, J.; Wu, R.; Huang, L.; Tan, L.; Chen, L.; Chen, Y. Fluorinated reduced graphene oxide as an efficient hole-transport layer for efficient and stable polymer solar cells. *ACS Omega* **2017**, *2*, 2010–2016. [[CrossRef](#)] [[PubMed](#)]
330. Liu, Z.; He, D.; Wang, Y.; Wu, H.; Wang, J. Graphene doping of P3HT: PCBM photovoltaic devices. *Synth. Met.* **2010**, *160*, 1036–1039. [[CrossRef](#)]
331. Robaey, P.; Bonaccorso, F.; Bourgeois, E.; D’Haen, J.; Dierckx, W.; Dexters, W.; Spoltore, D.; Drikkonigen, J.; Liesenborgs, J.; Lombardo, A.; et al. Enhanced performance of polymer: Fullerene bulk heterojunction solar cells upon graphene addition. *Appl. Phys. Lett.* **2014**, *105*, 083306. [[CrossRef](#)]
332. Jun, G.H.; Jin, S.H.; Lee, B.; Kim, B.H.; Chae, W.S.; Hong, S.H.; Jeon, S. Enhanced conduction and charge-selectivity by N-doped graphene flakes in the active layer of bulk-heterojunction organic solar cells. *Energy Environ. Sci.* **2013**, *6*, 3000. [[CrossRef](#)]
333. Bonaccorso, M.M.; Balis, F.; Stylianakis, N.; Savarese, M.; Adamo, C.; Gemmi, M.; Pellegrini, V.; Stratakis, E.; Kymakis, E. Functionalized Graphene as an Electron-Cascade Acceptor for Air-Processed Organic Ternary Solar Cells. *Adv. Funct. Mater.* **2015**, *25*, 3870–3880. [[CrossRef](#)]
334. Balis, N.; Konios, D.; Stratakis, E.; Kymakis, E. Ternary organic solar cells with reduced graphene oxide–Sb₂S₃ hybrid nanosheets as the cascade material. *ChemNanoMat* **2015**, *1*, 346–352. [[CrossRef](#)]
335. Dadashbeik, M.; Davood, F.; Mehdi, E. Design and simulation of perovskite solar cells based on graphene and TiO₂/graphene nanocomposite as electron transport layer. *Sol. Energy* **2020**, *207*, 917–924. [[CrossRef](#)]
336. Arefinia, Z.; Asghar, A. Optical and electrical modeling of solar cells based on graphene/Si nanowires with radial p–i–n junctions. *Sol. Energy Mater. Sol. Cells* **2015**, *137*, 146–153. [[CrossRef](#)]

Disclaimer/Publisher’s Note: The statements, opinions and data contained in all publications are solely those of the individual author(s) and contributor(s) and not of MDPI and/or the editor(s). MDPI and/or the editor(s) disclaim responsibility for any injury to people or property resulting from any ideas, methods, instructions or products referred to in the content.